DIFFUSION MRI CASE STUDY IN EPILESPY: A HEMISPHERIC REGIONAL BASED ANALYSIS OF DIFFUSION TENSOR IMAGING, TRACTOGRAPHY AND CONNECTOME IN PATIENTS WITH FOCAL AND GENETIC GENERALISED EPILEPSY

Kiki Hogenhuis
Department of Biomechanical Engineering
Technical University Delft

Supervisors
Prof. dr. Frans van der Helm
Dr. Mana Manoochehri
Department of Biomechanical Engineering
Techinical University Delft

In cooperation with
Stichting Epilepsie Intstellingen Nederland
Amsterdam AMC

February 17, 2020

ABSTRACT

Background: Imaging in the field of epilepsy has been a lasting challenge. In genetic generalised epilepsy (GGE) patients, conventional neuroimaging methods such as the MRI often appear normal and even in focal epilepsy (FE) an obvious structural abnormality is not always visualised. The objective of this exploratory case study is to identify white and grey abnormalities in epilepsy patients based on diffusion weighted imaging in comparison with healthy subjects.
Methods: Diffusion tensor imaging (DTI) and diffusion tensor tractography (DTT) at 3 Tesla is performed on 2 genetic generalised epilepsy patients, 1 focal epilepsy patient and 2 healthy subjects. Four DTI metrics (Fractional Anisotropy (FA), Mean Diffusivity (MD), Radial Diffusivity (RD) and Axial Diffusivity (AD) are compared based on the mean per region of interest between subjects and between hemispheres. A DTT map of the thalamo-cortical radiations is constructed based on a probabilistic tractography (iFOD2) as implemented in MRTrix. Based on this data the structural connectivity matrix is generated. A graph theoretical analysis is performed comparing node degree, global and local efficiency, characteristic path length, (average) clustering coefficient and (average) betweenness centrality. Constructed connectomes are compared for significant different connections between nodes using network based statistics.
Results: Decreased FA and MD values are reported in the hippocampus of the FE patient. DTT showed decreased tract density in the thalamo-cortical radiations in one of the GGE patients and the FE patient, together with a decreased mean streamline length compared to the two healthy subjects, which can be interpreted as a reduced structural connectivity. Structural connectivity is decreased in the FE patient compared to the other four subjects based on graph analysis. This is demonstrated by the relatively high average clustering coefficient and characteristic path length, together with a low node degree, high local efficiency and high clustering coefficient in the thalamus, the basal ganglia and the hippocampus.
Conclusion: These results are potentially of aid in identification of white and grey matter abnormalities in epilepsy patients. Especially in the FE brain several abnormalities in both DTI, DTT and graph analysis are observed compared to the healthy and GGE brain. However, for the use of DTI, DTT and graph analysis as a possible imaging biomarker, a standard processing pipeline with validated reference values ranges from the healthy population needs to be developed. Also the biological interpretation of changes in network measures needs to be validated.

***K*eywords** Epilepsy · Diffusion MRI · Tractography

Preface

Approximately one year ago I started with my graduation year. For my project I was situated at "Stichting Epilepsie Instellingen Nederland" (SEIN); a clinic based in Heemstede that focuses on the treatment and research in the field of epilepsy. Together with the researchers based at SEIN and my supervisors at the TU Delft, I started the exploratory study: Dynamic Information Flow based on EEG and diffusion MRI in subjects with epilepsy: an exploratory study. I dove into the world of epilepsy, (diffusion) MRI and transcranial magnetic stimulation (TMS). This document provides the outcomes of my work of the last year and is submitted in the fulfilment of the requirements for the degree of Msc Biomedical Engineering.

Epilepsy is a complex neurological disorder characterised by recurrent seizures. It is the most common serious neurological disorder worldwide, but there are still no reliable biomarkers [World Health Organization, 2019]. Recently renewed interest for the coupling of TMS with EEG (TMS-EEG) has grown among researchers to use it as an additional tool for epilepsy diagnostics and therapy evaluation. Recent studies have shown that epileptiform discharges are connected with changes in the dynamics of the brain and possible alterations in connectivity between interconnected areas of the brain [Siggiridou et al., 2014, Kugiumtzis et al., 2017, Shafi et al., 2016]. Transcranial magnetic stimulation (TMS) in combination with electroencephalogram (EEG) enables the non-invasive, direct study between brain areas. In the exploratory study we will try to evoke epileptogenic activity using TMS. The analysis will be done according to the Variational Bayesian Multimodal Encephalography (VBMEG) method to track the dynamic information flow in the epileptic brain after stimulation and compare this with healthy subjects. L. Filatova et al. [Filatova et al., 2018] demonstrated before the potential of the VBMEG method to capture cortical source activity and estimate dynamic information flow in neural networks in the brain. The application of network analysis in epilepsy provides valuable information on the seizure onset, propagation and termination, on the interictal state of functional networks and alterations in structural networks [Van Diessen et al., 2013].

The first step in medical scientific research involving human subjects is to write the study protocol for approval of the medical ethical committee (METC) to start the study. This includes among other things the study design, risk analysis and flyers and folders for participant information. A summary of the protocol is provided in Appendix 7.A. The second part involved a more detailed design of the experiment. During the experiment, an EEG registration with TMS is performed. With the use of a neuro-navigation system, five predefined markers are placed by a neurologist to define the location of the motor hand area on the precentral gyrus ("the hand knob"). During the experiment the definite location is determined, followed by a single pulse stimulation protocol. I wrote a standard operating procedure, so the experiment is reproducible for anyone that steps in after me. Thirdly, participants needed to be recruited. Together with my colleagues at SEIN, I recruited two genetic generalised epilepsy patients, one focal epilepsy patient and two healthy subjects after which we could start collecting data. The MRI scans were made at the Amsterdam Medisch Centrum (AMC). As we use a neuro-navigation system based on personal MRI's for TMS stimulation, the actual experiment can only take place after the MRI's are collected. Unfortunately, due to unforeseen circumstances it turned out that I could not execute the actual experiment I designed. Therefore, my article uses the data I had collected until that point, which were the five T1 and diffusion weighted MRI's.

Data analysis in this study is to be performed according to the VBMEG method, which aims to improve the spatial resolution of EEG for tracking the information flow inside the brain and it's changes following a TMS stimulation [Filatova et al., 2018]. In the VBMEG method anatomic and diffusion weighted MRI's are preprocessed, EEG sources are estimated using a hierarchical Variational Bayesian (hVB) approach. The linear connectome dynamics model is built by combining sources and anatomical connections extracted from diffusion MRI. Finally, this leads to the estimation of dynamic information flow travelling between sources [Filatova et al., 2018]. The workflow is schematically shown in figure 1.

Because the analysis of the MRI's in my study is part of the original project, my analysis largely follows the processing steps for (diffusion) MRI's as is proposed in the VBMEG method. Small adjustments and additions have been made in order to be able to make a comparison between subjects based on the diffusion and anatomical MRI's only, of which I have summarised the most important ones below:

- I have increased the number of streamlines from 100.000 to 10 million to create the tractography.
- I have used a more detailed atlas with more regions of interest (HCP MMP 1.0 Atlas [Glasser et al., 2016]) that is compatible with the MRtrix software toolbox.
- I have added the SIFT algorithm to correct for regions of crossing fibres [Smith and Tournier, 2013].

A detailed workflow of the analysis is added in the Appendix 7.E. Even though the number of subjects is small in this case study, still some remarkable differences between the epileptic and the healthy brain are found. Of which the two most important ones are the decreased FA and increased MD values in the hippocampus in the FE epilepsy

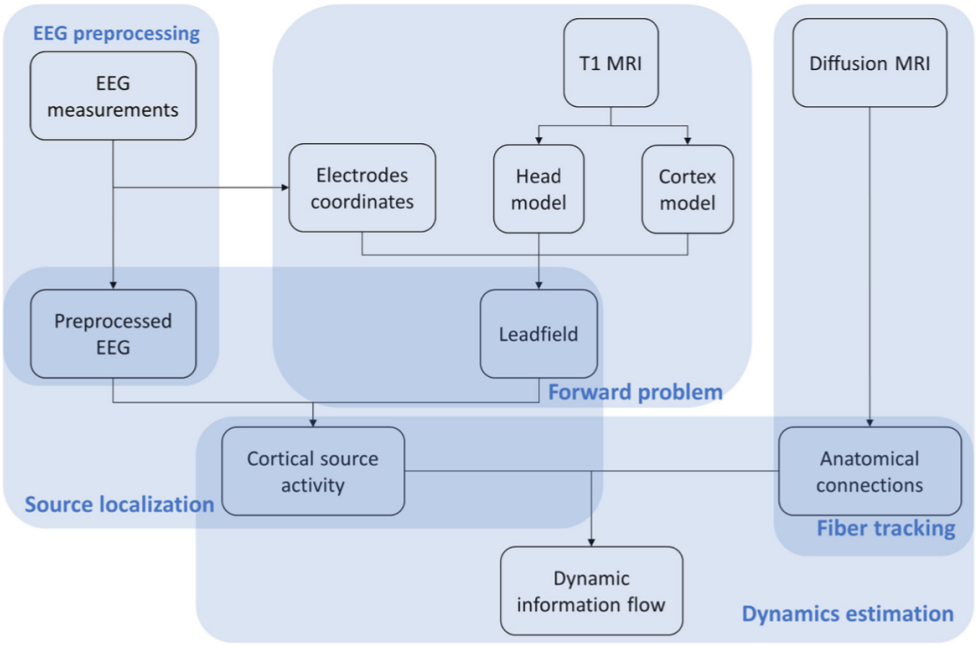

Figure 1: Workflow of the VBMEG method. "EEG, anatomic and diffusion weighted MRI's are first preprocessed. Then EEG sources are estimated using hVB approach. By combining sources and anatomical connections extracted from diffusion MRI, the linear connectome dynamics model is built leading to the estimation of dynamic information flow travelling between sources. The results are visualised individually for each subject dataset." Adapted from [Filatova et al., 2018]

patient, together with the decrease in streamline density in the thalamo-cortical tracts in two out of three epilepsy patients (1 GGE and 1 FE). The outcomes from this study already suggest an altered information flow in the epileptic brain compared to the healthy brain. In the future, by combining structural and physiological information from the T1- and diffusion-weighted MRI's and functional information from the EEG in the VBMEG method, we will be able to provide more information on several aspects of epilepsy, such as the seizure onset, propagation and termination, on the inter-ictal state of functional networks and on the alterations in structural networks in epilepsy patients compared to healthy subjects.

I want to thank Gerhard Visser, Robert Helling and Guido Widman at SEIN for their cooperation and help during my project. I have had a pleasant time doing research at the clinic and enjoyed the great amount of responsibility and authority they have given me. I have learned a lot from this project; how to think and write like a researcher, how to design a study and experiment, how to overcome hurdles along the way and lastly, not to be forgotten, is to have patience. Research takes time! At last, I want to give some special thanks to my supervisor Frans van der Helm and my daily supervisor Mana Manoochehri for their support and feedback.

Kiki Hogenhuis
February 17, 2020

Contents

1 Introduction

Approximately 50 million people worldwide are living with epilepsy according to the World Health Organisation. It is the fourth most common neurological disorder and affects people of all ages [**?**]. Considering the number of people suffering from epilepsy, a reliable tool for diagnostics would be of great value.

The current routinely used method used for diagnosis and seizure classification, the electroencephalogram (EEG), has its limitations in diagnostic yield and is often time-consuming. Besides EEG, magnetic resonance imaging (MRI) is an important tool in the process of diagnosing epilepsy. It can show the epileptic lesion and determine the presence and nature of the underlying pathology [Lee, 2010]. But, imaging in the field of epilepsy has been a lasting challenge. In genetic generalised epilepsy (GGE) patients, conventional neuro-imaging exams often appear normal [Yang et al., 2012]. Even in focal epilepsy, in many instances, an obvious structural abnormality is not visualised [Alizadeh et al., 2019]. Furthermore, in recent years, epilepsy has been conceptualised as a disorder involving networks, rather than a single source of pathology in the human brain. In both focal and generalised epilepsy, the brain network shows abnormalities in comparison with healthy brains. Recent evidence suggests involvement of brain areas far beyond the temporal lobe and into several regions bilaterally in temporal lobe epilepsy (TLE) patients [Richardson, 2012]. This has triggered the motivation to search for an additional tool for retaining more insight in the pathophysiology of epilepsy, for achieving a more effective way of diagnosing, treating and possibly a more personalised way of phenotyping epileptic diseases.

Among quantitative neuroimaging strategies, diffusion weighted imaging has the potential to identify grey and white matter abnormalities, including those that appear to be normal on the MRI. Advanced neuroimaging methods, such as diffusion tensor imaging (DTI) and diffusion tensor tractography (DTT), can be used to study the macroscopic structure

and structural connectivity in the human brain (the human connectome) [Alizadeh et al., 2019, Besson et al., 2014]. Several studies have showed structural damage in epilepsy patients based on DTI data such as fibre loss in the hippocampus and the limbic system [Luo et al., 2011, Peng et al., 2018, Bernhardt et al., 2015]. It has been hypothesised that seizure induced neuronal loss and axonal damage may lead to the development of aberrant connections between for example limbic structures [Spencer, 2002]. This might eventually result in the reorganisation of the network, thereby facilitating epileptogenicity and recurrent seizures [Spencer, 2002]. Therefore, the ability of DTI, DTT and network analysis to identify structural and network related abnormalities, has the potential to aid understanding of the acute and chronic pathophysiological effects of seizures on the brain, could lead to better disease quantification, prognosis assessment and therapy monitoring [Yogarajah and Duncan, 2008, Spencer, 2002, Bonilha et al., 2008].

The objective of this exploratory case study is to identify white and grey abnormalities in epilepsy patients based on diffusion weighted imaging in comparison with healthy subjects. DTI, DTT and graph theoretical analysis of structural network configuration is applied to diffusion weighted images from 3 patients with 2 different clinical scenarios and two healthy subjects. Two patients are diagnosed with a genetic generalised epilepsy (GGE) and 1 patient with focal epilepsy (FE) with underlying disease etiology mesiotemporal sclerosis (MTS), also commonly known as hippocampal sclerosis (HS). Outcomes are compared between hemispheres and with two healthy subjects. Note that until now, there are still no reference value ranges for DTI and DTT measures in healthy people [Alizadeh et al., 2019]. Previous studies have therefore compared between hemispheres, measurements or with a healthy control group. This study will try to delineate and identify abnormalities in the epileptic brain in comparison with the healthy brain to test for clinical and individual use as a possible biomarker.

2 Background

Water molecules placed inside a medium are in continuous motion because of their thermal energy. The human brain has a complex structure with neuronal axons, macro-molecules and cell membranes which hinder and restrict water diffusion. As a result, the water mobility is anisotropic. Since water diffusion occurs within and outside cellular structures, the degree of water diffusion in the brain provides a mean of probing cellular integrity and pathology [Le Bihan, 2003]. Diffusion weighted imaging (DWI) can measure the magnitude of diffusion within every voxel. By collecting multiple diffusion-weighted images with different encoding gradients, it is possible to characterise the three-dimensional pattern of water diffusion with a diffusion tensor model, incorporating information about the magnitude of diffusion at each point in the brain [Basser et al., 1994, Le Bihan et al., 2001]. The magnitude and preferred direction of the diffusion of water is described as the diffusion ellipsoid or tensor in every voxel. The tensor can be described by principle eigenvectors (x, y and z directions) with their corresponding eigenvalues ($\lambda_1, \lambda_2, \lambda_3$) (figure 2). The most common measures, based on the DTI model, are fractional anisotropy (FA), which describes the degree of anisotropy within a voxel and can be attributed to the orientation of the axon fibre, and the mean diffusivity (MD), which quantifies the magnitude of diffusion [Alizadeh et al., 2019]. The value of FA fluctuates between 0 (isotropic diffusion) and 1 (highly anisotropic). Reduction in FA represents the disorganisation of axon fibres, leading to unrestricted or isotropic diffusion. Increased MD indicates a disorganisation in structure [Douaud, 2014]. The hypothesis is that especially in regions with low FA values DTI could possibly be used as biomarker. Numerous studies report differences in epilepsy patients compared to healthy subjects [Chiang et al., 2016, Peng et al., 2018, Peng and Hsin, 2017, Luo et al., 2011]. Increased MD and decreased FA values in the hippocampus are reported in TLE patients, which could predict the lateralisation of the epileptogenic region [Chiang et al., 2016, Treit et al., 2019]. This change was related to the duration of epilepsy and is influenced by seizure recurrence. Other increases and decreases in FA have been found in regions such as the amygdala, corpus callosum, thalamus, striatum, accumbens and neocortex [Chiang et al., 2016, Lobato et al., 2018]. In generalised epilepsy patients DTI studies revealed structural abnormalities in the thalamus and basal ganglia [Lui et al., 2011, Luo et al., 2011, Zhang et al., 2011]. The "basal ganglia" refer to a group of sub-cortical nuclei which are primarily responsible for motor control and in the strictest sense refers to nuclei embedded deep in the brain hemispheres (nucleus caudatus, putamen and globus pallidus) [Lanciego et al., 2012]. The structural abnormalities in epilepsy patients can be directly related to the underlying etiology as the basal ganglia play an important role in seizure regulation [Berg et al., 2010]. Additionally, thalamo-cortical dysfunction is considered to be the major mechanism of GGE [Berg et al., 2010, Peng and Hsin, 2017, Yang et al., 2012]. These findings are also seen, but less often, in FE [Keller et al., 2011]. Abnormal interactions between the thalamus and the cortex cause generalised spike- and wave-discharges, although the definite origin of generalised epilepsy and roles of cortices and thalamus are still controversial [Zhang et al., 2011]. Other relevant scalar measures include axial diffusivity (AD) and radial diffusivity (RD), which can be interpreted as respectively myelin and axonal injury [Douaud, 2014]. This is particular of relevance in FE, as MTS or HS is the most common pathological substrate in temporal lobe epilepsy [Treit et al., 2019, Alizadeh et al., 2019]. Sclerosis means hardening or scarring, so in patients with MTS or HS, the hippocampus is damaged by neuronal cell loss and gliosis (a nonspecific reactive change of glial cells in response to damage to the central nervous system)

[Walker, 2015]. Concomitant abnormalities include granule cell dispersion, selective loss of inhibitory neurons, and axonal sprouting, which may together reflect a reorganisation of neuronal networks and explains the differences in FA, MD, RD and AD values compared to healthy subjects [Bernhardt et al., 2015].

Furthermore,the tensors calculated in DTI can be used to estimate the fibre orientation density function (fODF). One of the approaches to reconstruct fODF is by spherical deconvolution [Tournier et al., 2012]. Based on these fODF, tracts can be recreated in DTT; a visual and quantitative tool for reconstructing white matter tracts. In this study a probabilistic streamline tractography is used. The local fibre orientation density function (fODF) is interpret as a probability density distribution of the local fibre orientation. This technique yields maps that are related to the probability a certain voxel is connected to the starting point by randomly sampling this distribution many times and performing streamline tractography with each sample from always the same starting point (seed) [Jones, 2013].

Diffusion tensor metrics

Diffusion tensor
In an anisotropic, constrained environment:

$$Diffusiontensor(D) = D\overrightarrow{e_i} = \lambda_i \overrightarrow{e_i} \quad (1)$$

Fractional anisotropy (FA)

$$FA = \sqrt{\frac{3Var(\lambda)}{2(\lambda_1^2 + \lambda_2^2 + \lambda_3^2}} \quad (2)$$

Mean diffusivity (MD)

$$MD = \frac{\lambda_1 + \lambda_2 + \lambda_3}{3} \quad (3)$$

Axial diffusivity (AD)

$$AD = \lambda_1 \quad (4)$$

Radial diffusivity (RD)

$$RD = \frac{\lambda_2 + \lambda_3}{2} \quad (5)$$

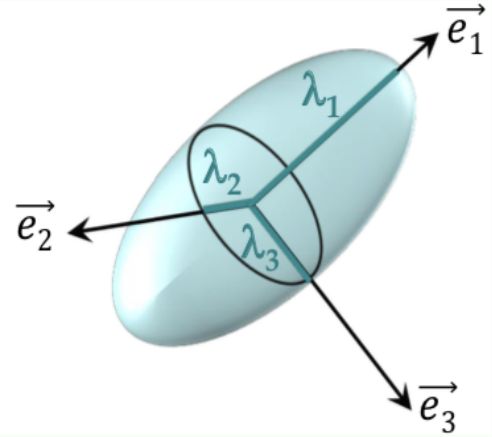

Figure 2: *Diffusion Ellipsoid.* Modified from [Douaud, 2014]

Based on the probabilistic tractography, a structural connectivity matrix is calculated and a connectome is constructed. As epilepsy has been conceptualised as a disorder involving networks, connectome analysis has gained much interest recently as a formal framework of quantitative network analysis [Besson et al., 2014]. In graph theory, nodes (brain areas) and edges (structural or functional connections between brain areas) form a network, enabling a mathematical analysis of the strength and efficacy between distant nodes [Besson et al., 2014]. The global organisation of the whole brain network is described in terms of node degree (the number of links connected to that node), clustering coefficient (which can be understood as the fraction of connected loops or triangles around a node), betweenness centrality (which represents the number of shortest paths from all nodes to all others that pass through that node, can be understood as the 'importance' of the node in the network), characteristic path length (the average shortest path length between all pairs of nodes in the network) and global efficiency (which represents the average inverse shortest path length in the network and be interpreted as a measure for effectiveness of information flow), which are in particularly relevant in the epileptic brain [Besson et al., 2014, Bonilha et al., 2008, Rubinov and Sporns, 2010]. A regular (or ordered) network has many local connections (high clustering coefficient), but a limited number of distant connections (and thus a high average path length) [Van Diessen et al., 2013]. In a random network it is the opposite: limited small connections and many distant connections. A small-world network combines the advantages of a regular network (good connectedness) with the advantages of a random network (good global connectedness) and is considered to be the most efficient network topology [Van Diessen et al., 2013]. Graph theoretical measures that are used in this study are summarised in table 1 and visualised in figure 4. Studies using EEG in patients with FE showed an increase in functional connectivity and a loss of network efficiency [Bartolomei et al., 2006, Horstmann et al., 2010, Van Dellen et al., 2012, Douw et al., 2010]. Studies investigating this loss of network efficiency reported an increased clustering coefficient and path length in patients with FE [Horstmann et al., 2010, Bernhardt et al., 2015]. Also Bernhardt and colleagues have reported an increased clustering coefficient and path length, while the small world topology largely remains preserved [Van Diessen et al., 2013, Bernhardt et al., 2015]. This was verified in the study of Bonilha and colleagues,

which showed structural reorganisation of the limbic areas, leading to aberrant connections and epileptogenicity [Bonilha et al., 2008].

Table 1: Graph theoretical measures that were investigated in this study. Adapted from [Bonilha et al., 2008] and [Rubinov and Sporns, 2010].

Graph theoretical measure	**Explanation**
Network measures	
Global efficiency	Average of inverse nodal shortest path
Average clustering coefficient	Average of nodal clustering coefficients
Average betweenness centrality	Average of nodal betweenness centrality
Characteristic path length	The average shortest path length in the network
Node measures	
Node degree	Number of links connected to that node
Local efficiency	Average of the inverse shortest path length in the neighbourhood of the node
Clustering coefficient	Fraction of a node's neighbours that are neighbours of each other
Betweenness centrality	Number of shortest paths from and to all nodes that pass this node

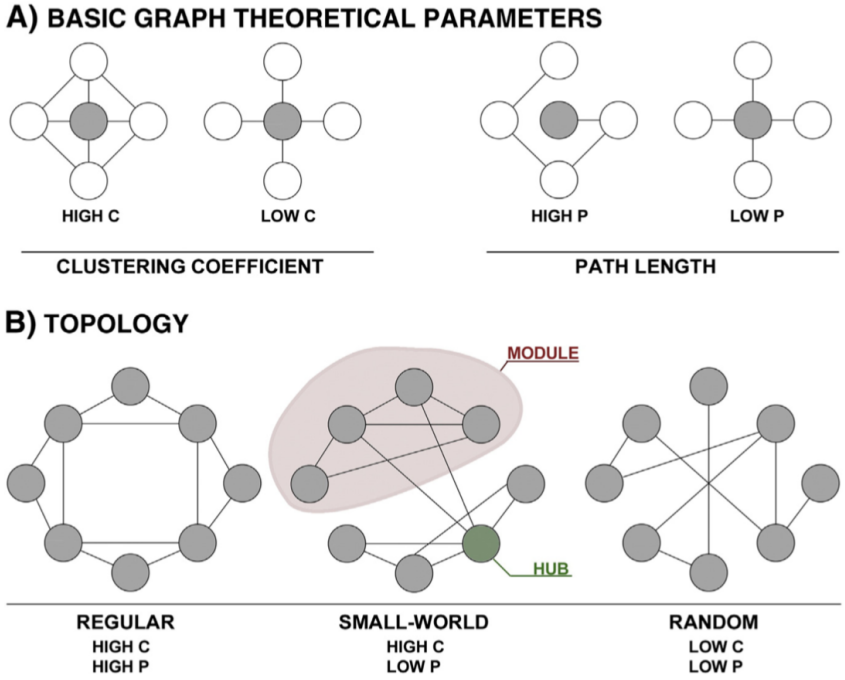

Figure 3: Graph theoretical measures. A) The clustering coefficient and path length are among the most used graph theoretical measures. Clustering measures the connection density of a given node among its neighbouring nodes. It relates o the local network efficiency and quantifies how robustly a network would compensate for the loss of a given node. The example shows a node with a high clustering coefficient and a node with a low clustering coefficient. The characteristic path length quantifies the average number of shortest paths between any two given nodes. The example contrasts a node with high path length to a node that has, on average, shorter path length to other nodes in the graph. B) Clustering coefficient and path length can characterise network topology. Regular networks have high clustering and path length; random networks have low clustering and path length. Small-world networks have clustering and path low path length and combine advantages from both regular and random. Modules (groups of densely interconnected nodes) and hubs (nodes with a high relevance for network connectivity) are frequently observed in small-world networks. Adapted from [Bernhardt et al., 2015]

3 Methods

3.1 Participants

The medical files of patients for EEG diagnostics at the epilepsy clinic 'Stichting Epilepsie Instellingen Nederland' (SEIN) are screened by neurologists. In this explorative study, a total of 5 participants (4 females, 1 male, 23-38 age range) have been included: 1 patient with FE, 2 patients with GGE, both according to standard clinical criteria, and 2 healthy control subjects. Patients were not included if they suffered from any other comorbidity's besides epilepsy. Clinical history of each of the patients can be found in Appendix 7.B. The study was approved by the Medical Ethical Committee (METC) of the Leiden University Medical Centre (LUMC). All methods were performed in accordance with the relevant guidelines and regulations approved by METC. Informed consent was obtained from all participants.

Table 2: Overview of participating subjects. HC=Healthy Control, GGE=Genetic Generalised Epilepsy, FE=Focal Epilepsy

Subject ID	Condition	Gender	Age	Seizure type	Medication
1	HC	Female	25		
2	HC	Female	32		
3	GGE	Female	23	Absence and tonic-clonic	Lamotrigine, Brivaracetam
4	GGE	Female	28	Absence (and tonic-clonic)	Lamotrigine, Levetiracetam
5	FE	Male	38	Focal and tonic-clonic	Carbamazepine, Clobazam, Lacosamide

3.2 Image acquisition

Subjects were scanned in a 3.0 Tesla Philips Scanner using an 8 channel head coil at the 'Academisch Medisch Centrum Amsterdam' (AMC). The T1-weighted images were acquired with a T1 MPRAGE sequence, using imaging parameters: FOV = 25.6 cm, voxel size = 1.0 x 1.0 x 1.0 mm3, matrix size = 256 x 256, TR = 12 ms, TE = 6 ms. DTI images were acquired axially using a single-shot echo planar imaging (EPI) sequence in the same anatomical location prescribed for T1-weighted images. The DTI parameters used were: FOV = 22.4 cm; diffusion weighted shells: b=1000 s/mm^2 (32 volumes), b=1700 s/mm^2 (48 volumes); number of reference scans (b0)= 1; voxel size = 2.33 x 2.33 x 2.33 mm3; matrix size = 96 x 96; TR = 7700 ms; TE 99 ms. The duration of the scanning session was approximately 20 minutes.

3.3 Data processing

DICOM images were converted into the NIFTI format and diffusion gradient directions were extracted with the software DCM2NII [Muschelli, 2019]. The raw data set of diffusion volumes were first correct for eddy current distortions using the FSL FDT diffusion toolbox and motion artefacts using FSL FLIRT (FMRIB's Linear Image Registration Tool) [Jenkinson et al., 2012]. Tools for eddy-current distortion correction and subject movement have not been systematically compared in this study, but research has shown that eddy provides a robust correction for eddy-current distortion and subject movement [Yamada et al., 2014]. Each directional diffusion image was aligned to the b0 volume (reference image). Eigenvalues ($\lambda 1, \lambda 2, \lambda 3$) and eigenvectors (v1, v2, v3) were computed from the pre-processed DTI volumes for each subject using FSL FDT diffusion toolbox. Four indices (FA, MD, RD and AD) were generated from the DWI image with b-value=1000.

T1-weighted images were preprocessed using SPM8 (`https://www.fil.ion.ucl.ac.uk/spm/`) and corrected for non-uniform intensities. Pre-processed images were processed with the Freesurfer suite (v6.) (`https://surfer.nmr.mgh.harvard.edu`), which provided skull stripping and grey/white matter segmentation. Subcortical grey matter structures were automatically segmentated. The grey and white matter was parcellated based on the HCP MMP 1.0 atlas which consists of 180 atlas regions in each hemisphere plus 19 subcortical regions [Glasser et al., 2016]. The subcortical regions correspond to the automatically segmentated regions from the Freesurfer reconstruction. Ten subcortical regions were selected as regions of interest (ROI) together with a neurologist. These regions include the cerebellum, thalamus, the basal ganglia (nucleus caudatus, putamen and globus pallidus), hippocampus, amygdala, accumbens, brain-stem, ventral DC. ROI's defined in T1 space were transformed into diffusion space where all calculations were made. All registrations were visually inspected to ensure their accuracy. Average DTI values (FA, MD, RD and AD) for each ROI were calculated and compared with the corresponding ROI in the opposite hemisphere and between subjects. A two-sample t-test is performed to test for significant differences between the left and right hemisphere per subject.

Additionally, anatomically constrained tract density imaging of the 379 atlas regions was generated. FOD was calculated using the response function based on the constrained spherical deconvolution model for multi-shell multi-

tissue (MSMT) data [Jeurissen et al., 2014]. Conventional single shell CSD is based only on white matter data. However, there are many voxels with "partial volumes", voxels contain besides white matter, also grey matter or CSF. By using MSMT data results in those regions are better estimated, since different tissue type are best sensitive for different b-values [Jeurissen et al., 2014]. 10 Million streamlines were generated by fibre orientation distribution (FOD) based probabilistic fibre tracking using the 2nd order Runge-Kutta method (iFOD2) as implemented in MRtrix version 3.0 (`https://www.mrtrix.org`). Anatomically-Constrained Tractography (ACT) correction is applied to ensure only anatomically feasible tracks are retained [Smith et al., 2012]. Optimised tracking parameters as proposed by MRtrix are used. The boundary between grey and white matter is used to create a mask for streamline seeding.

After the fibre-tracking, the spherical-deconvolution informed filtering of tracks (SIFT) algorithm was used to correct for bias in regions of crossing fibres [Smith and Tournier, 2013]. The SIFT algorithm reduces the number of streamlines from 10 million to 1 million and ensures the match between voxel-wise FOD and the streamlines count through each voxel. The streamlines connecting two regions are a proportional estimate of the cross-sectional area of the fibres connecting those two regions. The connectivity matrices of each subjects were built assigning the tracks to each node. The resulting structural connectivity matrix contained weighted connections between the 379 ROI. The weight assigned to each edge is defined by the average voxel-wise number of probabilistic fibre counts between regions. Results were compared with the contralateral side of the brain and between subjects. Based on the tractography, a tract density map is calculated, showing the apparent fibre density (AFD). A mask of the thalamus is created, and the thalamo-cortical radiations have been extracted. Figure 4 illustrates the processing pipeline. Results are visualised individually for each subject dataset.

Structural network properties were characterised using graph theory based measures from the brain connectivity toolbox for MATLAB [Rubinov and Sporns, 2010]. These graphical measures are directly calculated from the structural connectivity matrix. Measures investigated either relate to the global network properties (characteristic path length, network efficiency, average clustering coefficient and average betweenness centrality) and node properties (node degree, clustering coefficient, betweenness centrality and local efficiency). Every node corresponds to one of the predefined ROI. Measures used have a theoretical relationship with the network abnormalities that can be expected to be intrinsic to either GGE or FE [Bonilha et al., 2008]. The measures employed are summarised in table 1 [Bonilha et al., 2008]. Global differences in interconnected network components between patients and healthy subjects were performed with a statistical analysis of the resulting connectomes using the Network Based Statistics Package [Zalesky et al., 2010]. Two-sampled one-sided t-test with 50,000 permutations and threshold equal to 0.05 was employed.

4 Results

4.1 DTI findings

The mean values of FA, MD, RD and AD were calculated for ten predefined ROI (cerebellum, thalamus, nucleus caudatus, putamen, globus pallidus, hippocampus, amygdala, accumbens, brain-stem, ventral DC.) and compared with the corresponding ROI in the contra-lateral hemisphere and between subjects. Firstly, a lower FA value in the hippocampus combined with a higher MD is seen in the subject with focal epilepsy compared to the healthy subjects. Especially, ipsi-lateral to the sclerosis, the subject with focal epilepsy had the lowest FA value of all 5 participants. Both the GGE and FE patient(s) show relatively lower FA values and higher MD values compared to the healthy subjects in the thalamus. A left-right difference in FA values in the thalamus in subject 1 (HC), 3 (GGE) and 4 (GGE) is noticed (an increase of respectively 0.0191 and 0.0335 in the left thalamus with respect to right). Also in the basal ganglia (lower FA in the right nucleus caudatus compared to left and higher FA in the right globus pallidus compared to left) a difference between left and right is seen in subject 1, 3 and 4. A left-right difference is also seen in the FA values in the nucleus accumbens in subject 1, 3 and 4. Furthermore, in the amygdala a slightly higher FA and lower RD is noticed in all epilepsy patients compared to the healthy subjects. Lastly, the cerebellum has a decreased FA value and increased MD values in all three epilepsy patients. The tables for the RD and AD results can be found in Appendix 7.D. As these tables only provide complementary information to FA and MD, these tables are not included in the article.

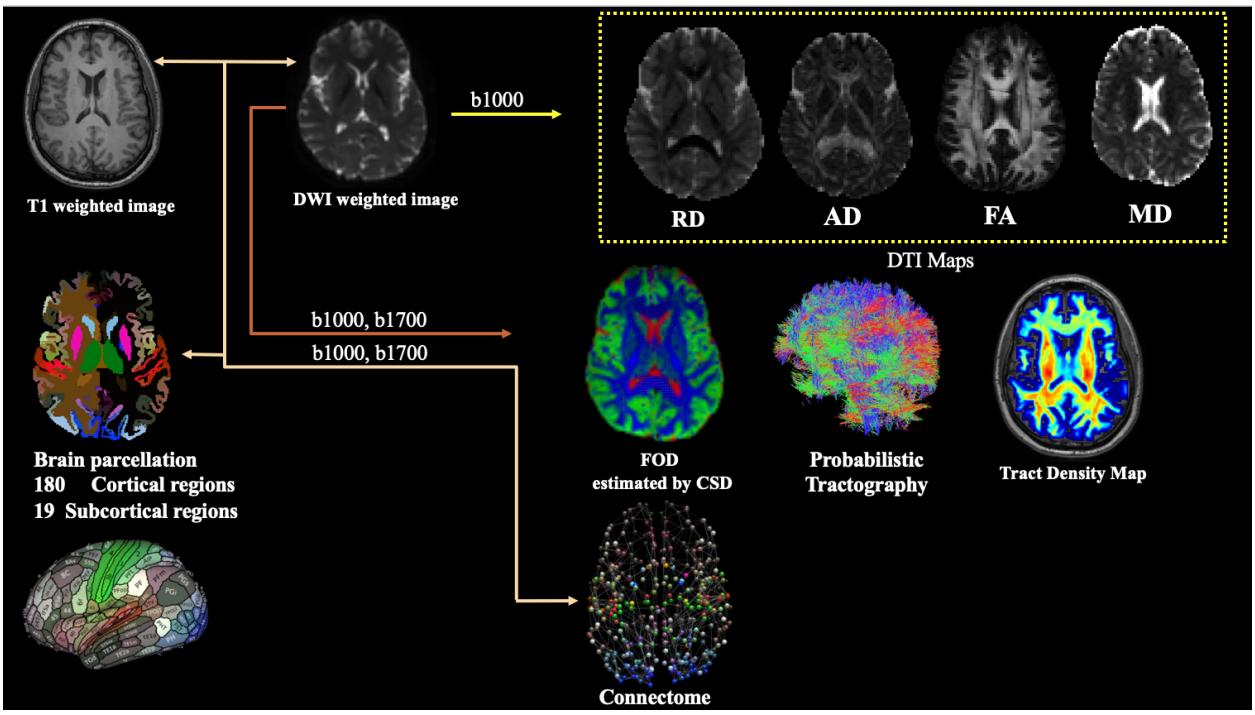

Figure 4: Illustration of the processing pipeline for the DTI, DTT and connectome analysis. The figure summarises maps derived from the T1-weighted image and diffusion weighted images. The b1000 images have been used to derive RD, AD, FA and MD maps. Both the b1000 and b1700 images have been used to perform a probabilistic tractography. The T1-weighted image has been used to create a (sub)cortical parcellation. This parcellation is combined with the diffusion data to construct the connectome.

Table 3: Mean fractional anisotropy (FA) values ± standard deviation per ROI per subject. The most important findings are highlighted in bold type. Ipsi-lateral to the sclerosis in the FE patient a lower FA compared to the healthy subjects is seen. The cerebellum has a decreased values in all three epilepsy patients. Left-right differences are present in the thalamus, nucleus caudatus, globus pallidus and nucleus accumbens of subject 1 (HC), 3 (GGE) and 4 (GGE). The HC=Healthy Control, GGE=Genetic Generalised Epilepsy, FE=Focal Epilepsy

Subject ID		**1 (HC)**	**2 (HC)**	**3 (GGE)**	**4 (GGE)**	**5 (FE)**
Cerebellum	Left	0.1815 ± 0.0922	0.1868 ± 0.0786	**0.1753 ± 0.0921**	**0.1660 ± 0.0762**	**0.1561 ± 0.0848**
	Right	0.1973 ± 0.1002	0.1972 ± 0.0768	**0.1852 ± 0.0951**	**0.1809 ± 0.0758**	**0.1672 ± 0.1014**
Thalamus	Left	**0.3215 ± 0.1368**	0.2863 ± 0.1092	**0.2769 ± 0.1053**	**0.2775 ± 0.1028**	**0.2506 ± 0.0909**
	Right	**0.2764 ± 0.0951**	0.2831 ± 0.1031	**0.2578 ± 0.1076**	**0.2440 ± 0.0909**	**0.2510 ± 0.0950**
Nucleus Caudutus	Left	**0.2633 ± 0.1428**	0.1972 ± 0.1064	**0.2365 ± 0.1351**	**0.2698 ± 0.1412**	0.2150 ± 0.1214
	Right	**0.1760 ± 0.0974**	0.1915 ± 0.1163	**0.1761 ± 0.1126**	**0.1513 ± 0.0743**	0.2008 ± 0.1077
Putamen	Left	0.2405 ± 0.1108	0.2114 ± 0.1091	0.2329 ± 0.1399	0.2371 ± 0.1177	0.2300 ± 0.1023
	Right	0.2743 ± 0.1571	0.2133 ± 0.1024	0.2581 ± 0.1571	0.2490 ± 0.1688	0.2496 ± 0.1020
Globus pallidus	Left	**0.2411 ± 0.1297**	0.3142 ± 0.1615	**0.3685 ± 0.2169**	**0.3017 ± 0.1472**	0.3417 ± 0.1930
	Right	**0.4922 ± 0.2273**	0.3315 ± 0.1517	**0.4878 ± 0.2408**	**0.4716 ± 0.2267**	0.3440 ± 0.1530
Hippocampus	Left	0.1620 ± 0.0757	0.1530 ± 0.0786	0.1597 ± 0.0917	0.1631 ± 0.0788	**0.1422 ± 0.0687**
	Right	0.1767 ± 0.1166	0.1490 ± 0.0777	0.1843 ± 0.1490	0.1753 ± 0.1133	**0.1474 ± 0.0643**
Amygdala	Left	0.1801 ± 0.0707	0.1754 ± 0.0619	0.1905 ± 0.0964	0.2058 ± 0.0825	0.1881 ± 0.0648
	Right	0.1782 ± 0.0854	0.1610 ± 0.0737	0.1906 ± 0.1203	0.1593 ± 0.0777	0.1758 ± 0.0619
Accumbens	Left	**0.2965 ± 0.1856**	0.2137 ± 0.0591	**0.3464 ± 0.1924**	**0.2542 ± 0.1310**	0.2476 ± 0.0902
	Right	**0.2394 ± 0.1229**	0.2200 ± 0.0632	**0.2505 ± 0.1395**	**0.2017 ± 0.0844**	0.2650 ± 0.1162

Table 4: Mean mean diffusivity (MD) value with standard deviation ($10^{-3}mm^2/s$) of selected ROI per subject. Important findings are highlighted in bold type. Increased values are seen in the cerebellum of all three epilepsy patients. Also the values in the hippocampus of the FE patient are increased. Left-right differences are present in the thalamus, nucleus caudatus, globus pallidus and nucleus accumbens of subject 1 (HC), 3 (GGE) and 4 (GGE). HC=Healthy Control, GGE=Genetic Generalised Epilepsy, FE=Focal Epilepsy

Subject ID		**1 (HC)**	**2 (HC)**	**3 (GGE)**	**4 (GGE)**	**5 (FE)**
Cerebellum	Left	0.8431 ± 0.4946	0.8712 ± 0.3976	**0.9329 ± 0.4954**	**0.9626 ± 0.5056**	**0.9114 ± 0.5652**
	Right	0.8663 ± 0.4782	0.8379 ± 0.3612	**0.9118 ± 0.4756**	**0.9140 ± 0.4424**	**0.9211 ± 0.5699**
Thalamus	Left	**0.7923 ± 0.1628**	0.8692 ± 0.2715	**0.9957 ± 0.4744**	**0.8641 ± 0.2952**	**0.9302 ± 0.3068**
	Right	**0.9929 ± 0.4805**	0.8757 ± 0.3126	**1.1245 ± 0.6154**	**1.0838 ± 0.5765**	**0.9860 ± 0.4342**
Nucleus Caudutus	Left	**0.7431 ± 0.1202**	0.9073 ± 0.3707	**0.7271 ± 0.0865**	**0.7769 ± 0.1284**	0.9207 ± 0.3921
	Right	**1.1809 ± 0.7349**	0.9401 ± 0.3346	**0.7004 ± 0.0627**	**1.3667 ± 0.7573**	1.0420 ± 0.5339
Putamen	Left	0.7654 ± 0.1369	0.7339 ± 0.0721	0.7271 ± 0.0865	0.7537 ± 0.1481	0.7439 ± 0.0898
	Right	0.7158 ± 0.1124	0.7370 ± 0.0809	0.7004 ± 0.0627	0.7325 ± 0.1038	0.7271 ± 0.1232
Globus pallidus	Left	**0.7884 ± 0.2115**	0.7298 ± 0.0978	**0.7227 ± 0.1015**	**0.7439 ± 0.1344**	0.7505 ± 0.1094
	Right	**0.6727 ± 0.0740**	0.7347 ± 0.0934	**0.6945 ± 0.0606**	**0.7008 ± 0.1119**	0.7486 ± 0.1317
Hippocampus	Left	1.0394 ± 0.3049	1.1146 ± 0.4309	1.2510 ± 0.6212	1.0759 ± 0.3891	**1.3313 ± 0.5702**
	Right	1.1191 ± 0.4404	1.0691 ± 0.3581	1.1488 ± 0.4608	1.0827 ± 0.4626	**1.1168 ± 0.4894**
Amygdala	Left	0.9221 ± 0.2675	0.9557 ± 0.3042	1.0404 ± 0.4245	0.9807 ± 0.2997	0.8706 ± 0.1522
	Right	0.9477 ± 0.3628	1.0003 ± 0.3384	0.9912 ± 0.3521	1.0014 ± 0.3496	0.9301 ± 0.3700
Accumbens	Left	**0.7679 ± 0.1205**	0.9388 ± 0.3166	**0.8156 ± 0.4231**	**0.8477 ± 0.2499**	0.8076 ± 0.1107
	Right	**0.8721 ± 0.2345**	0.8934 ± 0.1988	**0.8955 ± 0.3182**	**0.9632 ± 0.3141**	0.9465 ± 0.4017

4.2 DTT Findings

Figure 5 shows the tract density map of the thalamo-cortical radiations in the transverse plane. The pattern of both the healthy subjects is quite similar. While the pattern of subject 3 tends more towards the healthy subjects, the maps of both subject 4 and 5 are abnormal. Fewer and shorter tracts seem to evolve from the thalamus towards the cortex. But the thalamus itself shows a higher tract density compared to subject 1,2 and 3. When looking at the streamline length (table 5), the average is shorter in all three epilepsy patients compared to the healthy subjects

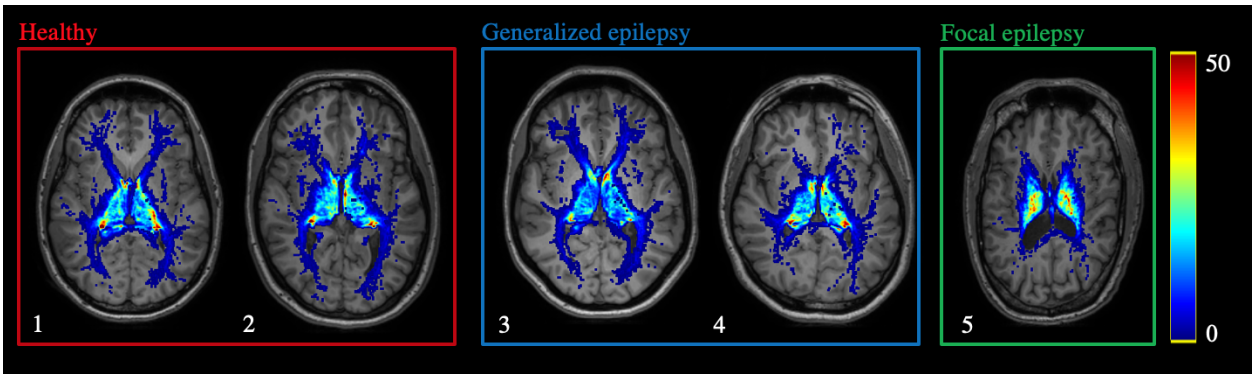

Figure 5: Cross-sectional images of the tract density maps from the thalamo-cortical radiations per subject in the transverse plane. Compared to the healthy subjects, the tract density is higher within the thalamus but lower in the radiations towards the cortex in the FE patient and in one of the GGE patients (subject 4).

Table 5: Mean streamline length (mm) in the thalamo-cortical radiations. HC=Healthy Control, GGE=Genetic Generalised Epilepsy, FE=Focal Epilepsy

Subject ID		**1 (HC)**	**2 (HC)**	**3 (GGE)**	**4 (GGE)**	**5 (FE)**
Mean Streamline length	Left	50.07 ± 33.40	50.97 ± 33.35	47.73 ± 33.66	53.59 ± 35.71	42.78 ± 29.30
	Right	50.79 ± 33.56	50.76 ± 44.41	45.93 ± 32.18	47.88 ± 35.12	38.07 ± 29.30

4.3 Topographic and network analysis

Global network properties (global efficiency, average clustering coefficient, average betweenness centrality and characteristic path length values) in the epileptic brain are compared to the two healthy subjects. The FE patient exhibited an increase in both average clustering coefficient and average betweenness centrality compared to both the generalised epilepsy patients and the healthy subjects. An increased characteristic path length is seen in subject 4 (GGE) and subject 5 (FE). Differences in global network efficiency did not stand out. The results of the node properties are visualised in figure 6. Subject 5 (FE) shows the lowest node degree in every region compared to the other four subjects, the differences are especially large in the cerebellum, thalamus, the basal ganglia and the hippocampus. An increased node degree in the pallidum in both the generalised epilepsy patients, subject 3 and 4 can be noticed compared to subject 1 (HC), 2 (HC) and 5 (FE). Furthermore, an increased local efficiency is noticed in focal epilepsy in the basal ganglia and the nucleus accumbens. The clustering coefficient is higher in subject 5 (FE) in the basal ganglia compared to the other subjects. Furthermore, the FE patient shows an increase in the nucleus accumbens, especially contra-lateral to the laesion (right hemisphere). Network based statistics did not show significant differences between subjects ($p >> 0.05$).

Table 6: Global network properties per subject. Important findings are shown in bold type. Subject 5 (FE) shows an increase in average clustering coefficient and average betweenness centrality. An increased characteristic path length is seen in subject 4 (GGE) and subject 5 (FE). HC=Healthy Control, GGE=Genetic Generalised Epilepsy, FE=Focal Epilepsy

Subject ID	**1 (HC)**	**2 (HC)**	**3 (GGE)**	**4 (GGE)**	**5 (FE)**
Global efficiency	0.0351	0.0354	0.0399	0.0322	0.0407
Average clustering coefficient	0.0039	0.0044	0.0042	0.0037	**0.0065**
Average betweenness centrality	767.46	767.55	766.98	748.18	**864.46**
Characteristic path length	0.0046	0.0047	0.0045	**0.0052**	**0.0054**

5 Discussion

This study tried to delineate and identify abnormalities in the grey and white matter of the epileptic brain in comparison with the healthy brain to test for clinical and individual use as a possible biomarker. Even with a small sample size DTI, DTT and graph analysis seems to have the potential to aid in identifying abnormalities in epilepsy.

In line with previously performed studies, the FA ROI analysis showed a decrease in the hippocampus in the FE patient ipsilateral to the sclerosis, combined with an increased MD [Salmenpera et al., 2006, Chiang et al., 2016, Nazem-Zadeh et al., 2014, Liacu et al., 2010, Focke et al., 2008, Thivard et al., 2005]. The increase in MD is merely due to an increase in RD, which confirms the myelin injury due to the sclerosis of the hippocampus. Especially in regions with low FA values, the bias for MD and FA measurements using ROI-based analysis is relatively small, which makes it possible to use it for diagnosing or response to the therapy in the brain as an imaging biomarker [Seo et al., 2019]. Recent studies suggest that the pathological changes seen in MTS reach beyond the sclerosis of the hippocampus and also involve structures located within the temporal lobes of the brain as well as neuronal connections projecting to other structures involving the limbic system [Inman and et al., 2018]. The involvement of the amygdala in the limbic system, might have caused the lower RD value in the ipsilateral amygdala, but no outstanding differences can be noticed in the FA and MD value. Discrepancy of the FA, MD, RD and AD findings may suggest differences in sensitivity to detect abnormalities with these measures [Lobato et al., 2018]. Many studies highlight the importance of the thalamus in generalised seizures [Kim et al., 2014, Peng and Hsin, 2017, Cunningham et al., 2017]. Generalised seizures occur in primary generalised epilepsy or can arise as a secondary generalisation [Peng et al., 2018]. Decreased FA values and increased MD values in the bilateral thalami are frequently reported [Peng et al., 2018]. Both the GGE and FE patient(s) show relatively lower FA values and higher MD values compared to the healthy subjects in the thalamus. The GGE patients show furthermore difference between left and right, in both cases the right thalamus has a relatively low FA together with a relatively high MD. The FA value in the thalamus is lower in subject 5 (FE) compared to subject 4 (GGE) and 5 (GGE). Keller and colleagues showed that the duration of epilepsy is negatively correlated with the mean FA of both the ipsilateral thamalus and the contralateral thalamus [Keller et al., 2011], which might explain the differences. The basal ganglia play an important role too in seizure regulation [Peng et al., 2018, Yang et al., 2012]. GGE patients have for example a smaller putamen compared to healthy people, with both microstructural and macrostructural abnormalities [Seeck et al., 2005]. Increased MD values bilaterally in the putamen and the left nucleus caudatus, along with increased FA values in the bilateral nucleus caudatus in patients with absence seizures are reported [Peng et al., 2018, Luo et al., 2011]. Both the GGE patients in this study suffer from absence seizures, but in contrast to Luo, subject 4 (GGE) shows) a lower MD in the left nucleus caudatus

Figure 6: Results from the graph theoretical analysis: node measures. The x-axis represents the defined ROI of interest: Cere=cerebellum, Thal=thalamus, Cau=nucleus caudatus, Put=putamen, Pall=pallidum, Hipp=hippocampus, Amyg=amygdala, Acc=nucleus accumbens, VDC=ventral DC, BS=brainstem. The horizontal line divides the graph into a left (left hemisphere) and right (right hemisphere) part. The y-axis represents the values for each of the four node measures. A) Node degree. The lowest values are seen in subject 5 (FE), especially in the thalamus, basal ganglia and the hippocampus. B) Local efficency. The highest values are seen in the basal ganglia of subject 5 (FE) and in the nucleus accumbens of subject 2 (HC) and 5 (FE). C) Clustering coefficient. The highest values are seen in the D) Betweenness centrality. The difference between left and right cerebellum is largest in subject 5(FE).

compared to the right nucleus caudatus, where the differences between left and right in subject 3 (GGE) are negligible. No increased MD values in the putamen are found. Also structural abnormalities in the cerebellum have been observed in patients with GGE and FE [Lui et al., 2011]. [Yang et al., 2012] showed increased MD values in bilateral cerebellar hemispheres, which in is accordance with the findings in this study where the MD values in the cerebellum of both the FE patient and the two GGE patients are increased compared to the healthy subjects.

DTT findings showed as tract density maps showed different patterns for the thalamo-cortical radiations in two out of three epilepsy patients. Early interictal diffusion imaging studies of patients with temporal lobe epilepsy have found structural disorganisation and expansion of extra cellular space, which is thought to reflect neuronal loss, reduction of dendritic branching and micro-structural changes associated with epileptogenisis [Yogarajah and Duncan, 2008, Assaf et al., 2003, Hak, 2005]. Also studies looking at generalised epilepsy find structural disorganisation in the thalamo-cortical radiations [Keller et al., 2011, Kim et al., 2014]. Thalamo-cortical radiations are essential in the generation of generalised seizures [Peng and Hsin, 2017]. Since the SIFT algorithm is applied, a weighted connectome is calculated that is more biologically relevant [Smith et al., 2015]. The number of streamlines connecting two areas of the grey matter is proportional to the total cross-sectional area of the white matter fibres connecting those areas. The tract density maps of subject 4 (GGE) and 5 (FE) show less fibres that reach the cortex with a lower density, while the tract density within the thalamus is higher. Also the mean lower average streamline length in subject 4 (GGE) and 5 (FE) confirms this and can be interpreted as reduced structural connectivity in the thalamo-cortical radiations. There exists a high degree of correspondence between structural and functional connectivity. Studies have reported that the functional connectivity within specific systems, is associated with the strength of the structural connectivity of the underlying white matter micro-structures based on the FA, MD and the radii of fibre bundles [Wang et al., 2014]. However, a strong structural connection does not directly mean that there exist a strong functional connection between regions and vice versa. This means that in order to assess connectivity in a reliable complete way, both functional and anatomical data is necessary. Lastly, the stability of these reconstructions rely on the number of generated streamlines, a greater number of streamlines may increase it's reproducibility and biological accuracy [Dhollander and Connely, 2014, Smith and Tournier, 2013].

Another way to look at structural connectivity is by assessing network properties using graph analysis. Even though analysis approaches have been relatively heterogeneous, consistent increases in both average clustering coefficient and characteristic path length have been reported in FE patients [Van Diessen et al., 2014]. Which is in accordance with the findings from subject 5 (FE). These findings suggest structural damage, in the form of neuronal loss and axonal damage, but do not tell whether there is an abnormal configuration of the network. It is suggested that these disruptions could result in the development of aberrant connections and eventually result in reorganisation of the network [Van Diessen et al., 2014]. FE is also associated with regional loss of connections. This is demonstrated by a reduction in structural connectivity between regions, which is reflected in a decreased node degree in the thalamus, the basal ganglia and the hippocampus in subject 5 (FE). Lastly a higher clustering coefficient in the limbic system and a higher influence of specific nodes over the network is reported [Bonilha et al., 2008]. Which is in contrast to the value of the clustering coefficient in the hippocampus in subject 5 (FE), as the difference with the other subjects is very small. Also in GGE patients abnormalities with regard to network properties have been reported. Among these are an increased characteristic path length and reduced local and global efficiencies, which indicates low connectivity, disorganisation and reduced efficiency of the network [Xue et al., 2014]. Apart from the increased characteristic path length in subject 4 (GGE), the outcomes from the graph analysis in this study did not align with previous studies [Bonilha et al., 2008, Besson et al., 2014, Xue et al., 2014]. Decreased structural connections are reported among the sub-cortical nuclei, therefore differences were also expected in the thalamus, hippocampus and basal ganglia, but global network as well as node measures were comparable between healthy and generalised epilepsy patients. Analysis based on individual assessment has small power, this is confirmed by the lacking of any significant differences between networks using networks based statistics. It must be noted that the relationship between these structural network changes and clinical manifestations of epilepsy are not clear yet [Bernhardt et al., 2015]. Furthermore, previous studies have been giving contradicting results, partly due to the variability in the definition of nodes, the determination of edges, and the choice of graph theoretical parameters analysed [Bonilha et al., 2008, Bernhardt et al., 2015, Taylor et al., 2014, Besson et al., 2014, Xue et al., 2014].

When comparing all three analyses; DTI, DTT maps and graph analysis between the healthy subjects and epilepsy patients, the outcomes of subject 3 (GGE) tend to look more like the healthy subjects, compared to subject 4 (GGE) and 5 (FE). As the duration of epilepsy is positively related to the damage in the brain, the longer disease duration of subject 4 (GGE, diagnosed in 2007) and 5 (FE, diagnosed in 2009), compared to subject 3 (GGE, diagnosed 2015) could partly explain the differences [Peng et al., 2018]. It should be noted though, that the year of diagnosing does not necessarily mean that the patient has not been suffering from epilepsy for a longer time. Also the frequency of the seizures and chronic use of AED's may affect the results the study [Van Dellen et al., 2009, Van Dellen et al., 2012]. Besides these,

other general modifiers such as intellectual performance and state of vigilance may have had effect on the outcomes [Van Diessen et al., 2013].

Even though discussed results are mostly in accordance with previously published studies, the results of this study need to be read with caution. Discrepancies with previous findings from other studies may have resulted from the low sample size in this study. It cannot be stated that the two healthy subjects are a reliable representation of the healthy population. Therefore, significant differences may be detected with larger samples. Furthermore, since there are no reference values and standardised processing guidelines for DTI and DTT available, direct comparison with other studies is at this moment not possible. Analysis approaches in network analysis have been relatively heterogeneous, both with respect to patient inclusion criteria, network construction methods, and the choice of theoretical measures [Bernhardt et al., 2015]. There is no overarching agreement about which parcellation scheme and spatial scale provide the most adequate definition of network nodes to describe and interpret network properties [Bernhardt et al., 2015], which means that biological interpretation of network analysis still remains difficult. Additionally, DTI has methodological limitations. The metrics are among other things as accurate as the quality of the image; the smaller the voxel the more precise and anatomically trustworthy the image. Due to the size of the voxels, it is likely that a single voxel will contain numerous fibres which do not have the same orientation. Furthermore, as the outcomes of both DTI and DTT as well as graph analysis highly depend on the processing pipeline, various factors needs to be taken into consideration like the definition of the ROI, the atlas that is used, effects of motion, registration and spatial normalisation.

6 Conclusion

DTI and DTT analysis has the potential to aid in identification of white and grey matter abnormalities in epilepsy patients. The following promising results may be developed into imaging biomarkers:

- Decreased FA and MD values are reported in the hippocampus of subject 5 (FE). This aligns with the hypothesis that especially in regions with low FA values DTI could possibly be used as biomarker.
- DTT showed decreased tract density in the thalamo-cortical radiations in subject 4 (GGE) and subject 5(FE), together with a decreased mean streamline length compared to subject 1 (HC), 2 (HC) and 3 (GGE), which can be interpreted as a reduced structural connectivity.
- Structural connectivity is decreased in subject 5 (FE) compared to the other four subjects based on graph analysis. This is demonstrated by the relatively high average clustering coefficient and characteristic path length, together with a low node degree, high local efficiency and high clustering coefficient in the thalamus, the basal ganglia and the hippocampus.

However, for the use of DTI, DTT and graph analysis in a clinical setting as a possible biomarker, a standard processing pipeline with validated reference values ranges from the healthy population needs to be developed. Also the biological interpretation of changes in network measures needs to be analysed. In this study no definite conclusion can be drawn about differences between an epileptic and a healthy brain based on DTI metrics. Nonetheless, these preliminary results are encouraging and warrant additional research with a larger sample size.

6.1 Future recommendations

In the future it will be beneficial to acquire DTI at a higher field strength, with improved radiofrequency coils and multiband DTI techniques, which will allow for the imaging of small voxels while still maintaining a relatively short imaging time [Alizadeh et al., 2019]. The optimal number of diffusion directions is not determined yet and depends on different factors like the robustness of the post processing algorithms, voxel size, reasonable acquisition time for clinical applications and scan parameters (e.g. TE) [Alizadeh et al., 2019, Tournier et al., 2012]. Additionally, by combining different imaging modalities, we may improve our understanding of the brain as a complex biological system. This will help to interpret the differences between healthy subjects and epilepsy patients and eventually to use these differences as biomarkers. Hypotheses about altered structure-function relationship and assumptions about epilepsy as a network disorder can be assessed. For example, by combining functional MRI (fMRI) and DTI techniques information about the functional impact of white matter tract abnormalities can be evaluated. Additionally, new methods of data analysis may be helpful in combined analysis of different techniques. Connectivity analysis in epilepsy patients can provide information on several aspects such as the seizure onset, propagation and termination, on the inter-ictal state of functional networks in epilepsy and on the alterations in structural networks [Braun and van Diessen, 2013]. In a future exploratory study we will apply the Variational Bayesian Multimodal Encephalography method to combine structural, physiological and functional information from EEG and MRI measurements to estimate the dynamic interactions between active sources, i.e. effective connectivity [Filatova et al., 2018].

References

[Hak, 2005] (2005). Apparent diffusion coefficient measurements in the hippocampus and amygdala of patients with temporal lobe seizures and in healthy volunteers. *Epilepsy Behav*, (6):250–256.

[Alizadeh et al., 2019] Alizadeh, M., Kozlowski, L., Ashraf, N., and Shahrampour, S. (2019). Hemispheric regional based analysis of diffusion tensor imaging and diffusion tensor tractography in patients with temporal lobe epilepsy and correlation with patient outcomes. *Nature Scientific Report 9:215*.

[Assaf et al., 2003] Assaf, B., Mohamed, F., Abou-Khaled, K., Williams, J., Yazeji, M.S. Haselgrove, J., and Faro, S. (2003). Diffusion tensor imaging of the hip- pocampal formation in temporal lobe epilepsy. *AJNR Am J Neuroradiol*, (24):1857–1862.

[Bartolomei et al., 2006] Bartolomei, F., Bosma, I., Klein, M., Baayen, J., Reijneveld, J., and T.J., P. (2006). Disturbed functional connectivity in brain tumour patients: evaluation by graph analysis of synchronization matrices. *Clin Neurophysiol*, (117):2039–2049.

[Basser et al., 1994] Basser, P., Matiello, J., and Le Bihan, D. (1994). Estimation of the effective self-diffusion tensor from the nmr spin echo. *J Magn Reson B 103*, pages 247–254.

[Berg et al., 2010] Berg, A., Berkovic, S., and Brodie, M. (2010). Revised terminology and concepts for organization of seizures and epilepsies: report of the ilae commission on classification and terminology. *Epilepsia: 51;4*, pages 676–685.

[Bernhardt et al., 2015] Bernhardt, B., Bonilha, L., and Gross, D. (2015). Network analysis for a network disorder: The emerging role of graph theory in the study of epilepsy. *Epilepsy Behavior*.

[Besson et al., 2014] Besson, P., Dinkelacker, V., Valabregue, R., and Thivard, L. (2014). Structural connectivity differences in left and right temporal lobe epilepsy. *NeuroImage: 100*, pages 135–144.

[Bonilha et al., 2008] Bonilha, L., Nesland, T., and Martz, G. (2008). Medial temporal lobe epilepsy is associated with neuronal fibre loss and paradoxical increase in structural connectivity of limbic structures. *Neuroimage: 42;2*, pages 515–524.

[Braun and van Diessen, 2013] Braun, K. and van Diessen, S. (2013). Functional and structural brain networks in epilepsy. what have we learned? *Epilepsia: 54*, pages 1855–1865.

[Chiang et al., 2016] Chiang, S., Levin, H., and Wilde, E. (2016). White matter structural connectivity changes correlate with epilepsy duration in temporal lobe epilepsy. *Epilepsy: 120;1*, pages 37–46.

[Cunningham et al., 2017] Cunningham, S., Tomasi, D., and Volkow, N. (2017). Structural and functional connectivity of the precuneus and thalamus to the default mode network. *Human Brain Mapping*, (38):938–956.

[Dhollander and Connely, 2014] Dhollander, T. and Connely, A. (2014). Generating a t1-like contrast using 3-tissue constrained spherical deconvolution results from single-shell (or multi-shell) diffusion mr data. *Conf. ISMRM Work. Break. Barrier. Diffus. MRI*.

[Douaud, 2014] Douaud, G. (2014). Practical analysis and interpretation: Dti and tractography.

[Douw et al., 2010] Douw, L., de Groot, M., van Dellen, E., Heimans, J., Ronner, H., Stam, C., and Reijneveld, J. (2010). 'functional connectivity' is a sensitive predictor of epilepsy diagnosis after the first seizure. *PLoS ONE*, (5):e10839.

[Engel, 2008] Engel, J. (2008). Progress in epilepsy: reducing the treatment gap and the promise of biomarkers. *Curr Opin Neurol*, 2(21):150–154.

[Filatova et al., 2018] Filatova, O., Yang, Y., Dewald, J., and Tian, R. (2018). Dynamic information flow based on eeg and diffusion mri in stroke: A proof-of-principle study. *Frontiers in Neural Circuits: 12;79*.

[Focke et al., 2008] Focke, N., Yogarajah, M., Bonelli, S., Bartlett, P., Symms, M., and Duncan, J. (2008). Voxel-based diffusion tensor imaging in patients with mesial temporal lobe epilepsy and hippocampal sclerosis. *NeuroImage*, (40):728–737.

[Glasser et al., 2016] Glasser, M., Coalson, T., Robinson, E., Hacker, C., and Harwell, J. (2016). A multi-modal parcellation of human cerebral cortex. *Nature: 536*, pages 171–178.

[Horstmann et al., 2010] Horstmann, M., Bialonski, S., Noennig, N., Mai, H., Prusseit, J., Wellmer, J., H., H., and Lehnertz, K. (2010). State dependent properties of epileptic brain networks: comparative graph-theoretical analyses of simultaneously recorded eeg and meg. *Clin Neurophysiol*, (121):172–185.

[Inman and et al., 2018] Inman, C. and et al. (2018). Direct electrical stimulaion of the amugdala enhances declarative memory in humans. *Proc Natl Acad Sci USA: 115*, pages 98–103.

[Jenkinson et al., 2012] Jenkinson, M., Beckmann, C., Behrens, T., Woolrich, M., and Smith, S. (2012). Fsl. *NeuroImage: 62*, pages 782–790.

[Jeurissen et al., 2014] Jeurissen, B., Tournier, J., Dhollander, T., and Connelly, A. (2014). Multi-tissue constrained spherical deconvolution for improved analysis of multi-shell diffusion mri data. *NeuroImage: 103*, pages 411–426.

[Jones, 2013] Jones, D. (2013). White matter integrity, fiber count, and other fallacies: The do's and don'ts of diffusion mriv. *NeuroImage*, (73):239–254.

[Keller et al., 2011] Keller, S., Ahrens, T., Mohammadi, S., Moddel, G., Kugel, H., Ringelstein, E., and Deppe, M. (2011). Microstructural and volumetric abnormalities of the putamen in juvenile myoclonic epilepsy. *Epilepsia*, (52):1715–1724.

[Kim et al., 2014] Kim, J., Suh, S., Seo, W., Oh, K., and Koh, S. (2014). Altered thalamocortical functional connectivity in idiopathic generalized epilepsy. *Epilepsia*, (55(4)):592–600.

[Kugiumtzis et al., 2017] Kugiumtzis, D., Koutlis, C., and Tsimpiris, A. (2017). Dynamics of epileptiform discharges induced by transcranial magnetic stimulation in genetic generalized epilepsy. *Int. J. of Neural Systems*, 7(27).

[Lanciego et al., 2012] Lanciego, J., Luquin, N., and Obeso, J. (2012). Functional neuroanatomy of the basal ganglia. *Cold Spring Harb Perspect Med.*, 12(2):a009621.

[Le Bihan, 2003] Le Bihan, D. (2003). Looking into the functional architecture of the brain with diffusion mri. *Nat Neurosci: 4*, pages 534–546.

[Le Bihan et al., 2001] Le Bihan, D., Mangin, J., Poupon, C., and et al. (2001). Diffusion tensor imaging: concepts and applications. *J Magn Reson Imaging 13*, pages 534–546.

[Lee, 2010] Lee, G. (2010). *Neuropsychology of Epilepsy and Epilepsy Surgery*. Oxford University Press.

[Liacu et al., 2010] Liacu, D., de Marco, G., Ducreux, D., Bouilleret, V., Masnou, P., and I., I.-P. (2010). Diffusion tensor changes in epileptogenic hippocampus of tle patients. *Clin Neurophysiol*, (40):151–157.

[Lobato et al., 2018] Lobato, M., Garciab, L., Amaro Jrb, E., Otaduyb, M., Jorgea, C., and Castroa, L. (2018). Analysis of fractional anisotropy and mean diffusivity in refractory and non- refractory idiopathic generalized epilepsies. *European Journal of Epilepsy*, pages 33–37.

[Lui et al., 2011] Lui, M., Concha, L., and Beaulieau, C. (2011). Distinct white matter abnormalities in different idiopathic generalized epilepsy syndromes. *Epilepsia: 52;12*, pages 2267–275.

[Luo et al., 2011] Luo, C., Xia, Y., and Li, Q. (2011). Diffusion and volumetry abnormalities in subcortical nuclei of patients with absence seizures. *Epilepsia: 52;6*, pages 1092–1099.

[Muschelli, 2019] Muschelli, J. (2019). *dcm2niir: Conversion of 'DICOM' to 'NIfTI' Imaging Files Through R*. R package version 0.6.9.1.

[Nazem-Zadeh et al., 2014] Nazem-Zadeh, M., Schwalb, J., Elisevich, K., H., B.-E., Hamidian, H., and Akhondi-Asl, A. (2014). Lateralization of temporal lobe epilepsy using a novel uncertainty analysis of mr diffusion in hippocampus, cingulum, and fornix, and hippocampal volume and flair intensity. *J Neurol Sci*, (71):152–161.

[Peng et al., 2018] Peng, S., Harnod, T., Tsai, J., Ker, M., and et al. (2018). Evaluation of subcortical grey matter abnormalities in patients with mri-negative cortical epilepsy determined through structural and tensor magnetic resonance imaging. *Proc Natl Acad Sci USA: 115*, pages 98–103.

[Peng and Hsin, 2017] Peng, S. and Hsin, Y. (2017). Altered structural and functional thalamocortical networks in secondarily generalized extratemporal lobe seizures. *NeuroImage*, (Clinical 13):55–61.

[Richardson, 2012] Richardson, J. (2012). Large scale brain models of epilepsy: dynamics meets connectomics. *J Neurol Neurosurg Psychiatry*.

[Rubinov and Sporns, 2010] Rubinov, M. and Sporns, O. (2010). Complex network measures of brain connectivity: Uses and interpretations. *NeuroImage: 52;3*, pages 1059–1069.

[Salmenpera et al., 2006] Salmenpera, T., Simistera, R., Barletta, P., Symmsa, M., P.A., B., Freea, S., Barker, G., and J.S., D. (2006). High-resolution diffusion tensor imaging of the hippocampus in temporal lobe epilepsy. *Epilepsy Research*, (71):102–106.

[Seeck et al., 2005] Seeck, M., Dreifuss, S., Lantz, G., Jallon, P., Foletti, G., Despland, D., Delavelle, J., and Lazeyras, F. (2005). Subcortical nuclei volumetry in idiopathic generalized epilepsy. *Epilepsia*, (46(10)):1642–1645.

[Seo et al., 2019] Seo, Y., Rolling, N., and Wang, Z. (2019). Reduction of bias in the evaluation of fractional anisotropy and mean diffusivity in magnetic resonance diffusion tensor imaging using region-of-interest methodology. *Nature Research - Scientific Report*, (13095).

[Shafi et al., 2016] Shafi, M., Whitfield-Gabrieli, S., and Chu, C. (2016). A multimodel imaging- and stimulation-based method of evaluating connectivity-related brain excitability in patients with epilepsy. *Journal of Visualised Experiments*, (117).

[Siggiridou et al., 2014] Siggiridou, E., Kugiumtzis, D., and Kimiskidis, V. (2014). Correlation networks for identifying changes in brain connectivity during epileptiform discharges and transcranial magnetic stimulation. *Sensors*, (14):12585–12597.

[Smith and Tournier, 2013] Smith, R. and Tournier, J. (2013). Spherical-deconvolution informed filtering of tractograms. *Proc. Intl. Soc. Mag. Reson. Med. 20*.

[Smith et al., 2012] Smith, R., Tournier, J., Calamante, F., and Connely, A. (2012). Anatomically-constrained tractography: Improved diffusion mri streamlines tractography through effective use of anatomical information. *NeuroImage*, (62):1924–1938.

[Smith et al., 2015] Smith, R., Tournier, J., Calamante, F., and Connely, A. (2015). The effects of sift on the reproducibility and biological accuracy of the structural connectome. *NeuroImage*, (104):253–265.

[Spencer, 2002] Spencer, S. (2002). Neuronal networks in human epilepsy: evidence of and implications for treatment. *Epilepsia*, (43):219–227.

[Tahedi, 2018] Tahedi, M. (2018). Batman - basic and advanced tractography with mrtrix for all neurophiles.

[Taylor et al., 2014] Taylor, P., Kaisera, M., and Dauwels, J. (2014). Structural connectivity based whole brain modelling in epilepsy. *Journal of Neuroscience Methods*, (236):51–57.

[Thivard et al., 2005] Thivard, L., Lehericy, S., Krainik, A., Adam, C., Dormont, D., and Chiras, J. (2005). Diffusion tensor imaging in medial temporal lobe epilepsy with hippocampal sclerosis. *NeuroImage*, (28):682–690.

[Tournier et al., 2012] Tournier, J., Calamante, F., and Connell, Y. (2012). Mrtrix: Diffusion tractography in crossing fiber regions. *International Journal of Imaging Systems and Technology*, pages 53–66.

[Treit et al., 2019] Treit, S., Little, G., Steve, T., Nowacki, T., Schmitt, L., Weathley, B., and Beaulieau, M. (2019). Regional hippocampal diffusion abnormalities associated with subfield-specific pathology in temporal lobe epilepsy. *Epilepsia Open*, (4):544–554.

[Van Dellen et al., 2009] Van Dellen, E., Douw, L., and Baayen, J. (2009). Long-term effects of temporal lobe epilepsy on local neural networks: A graph theoretical analysis of corticography recordings. *PLoS ONE*, 4(11).

[Van Dellen et al., 2012] Van Dellen, E., Douw, L., and Hillebrand, A. (2012). Meg network differences between low- and high-grade glioma related to epilepsy and cognition. *PloS ONE*, 7(e50122).

[Van Diessen et al., 2013] Van Diessen, E., Diederen, S., and Braun, K. (2013). Functional and structural brain networks in epilepsy. what have we learned? *Epilepsia*, 54(11):1855–1865.

[Van Diessen et al., 2014] Van Diessen, E., Zweiphenning, W., Jansen, F., Stam, C., Braun, K., and Otte, W. (2014). Brain network organizaation in focal epilepsy: a systematic review and meta-analysis. *PLoS One*, (9):e114606.

[Walker, 2015] Walker, C. (2015). Hippocampal sclerosis: Causes and prevention. *Semin Neurol*, 35(3):193–200.

[Wang et al., 2014] Wang, J., Qui, S., Xu, Y., Liu, Z., Wen, X., Hu, X., Zhang, R., and Li, M. (2014). Graph theoretical analysis reveals disrupted topological properties of whole brain functional networks in temporal lobe epilepsy. *Clinical Neuropsychology*, (125):1744—1756.

[World Health Organization, 2019] World Health Organization (2019). Chapter 1: Global burden of epilepsy. *Epilepsy: A public health imperative*, pages 9–17.

[Xue et al., 2014] Xue, K., Luo, C., Zhang, D., Yang, T., J., L., Gong, D., Chen, L., Medina, Y., Gotman, J., Zhou, D., and Yao, D. (2014). Diffusion tensor tractography reveals disrupted structural connectivity in childhood absence epilepsy. *Epilepsy Research*, (108):125–138.

[Yamada et al., 2014] Yamada, H., Abe, O., and Shizukuishi, T. (2014). Efficacy of distortion correction on diffusion imaging: Comparison of fsl eddy and eddy$_{c}orrectusing30and60directionsdiffusionencoding.PloSOne.$

[Yang et al., 2012] Yang, T., Guo, Z., Luo, C., Li, Q., and et al. (2012). White matter impairment in the basal ganglia-thalamocortical circuit of drug-naive childhood absence epilepsy. *Epilepsy Res: 99*, pages 267–273.

[Yogarajah and Duncan, 2008] Yogarajah, M. and Duncan, J. (2008). Diffusion-based magnetic resonance imaging and tractography in epilepsy. *Epilepsia: 49;2*, pages 189–200.

[Zalesky et al., 2010] Zalesky, A., Fornito, A., and Bullmore, E. (2010). Network-based statistics: Identifying differences in brain networks. *NeuroImage: 53*, pages 1197–1207.

[Zhang et al., 2011] Zhang, Z., Liao, W., and Chen, W. (2011). Altered functional-structural coupling of large-scale brain networks in idiopathic generalized epilepsy. *Brain: 134;Pt 10*, pages 2912–2928.

7 Appendix

7.A Summary Study Protocol

A summary of the protocol of the study: Dynamic Information Flow based on EEG and diffusion MRI in subjects with epilepsy: an exploratory study.

Rationale

Epilepsy is a complex neurological disorder characterised by recurrent seizures. It is the most common serious neurological disorder worldwide, but there are still no reliable biomarkers. Recently renewed interest for the coupling of TMS with EEG (TMS-EEG) has grown among researchers to use it as an additional tool for epilepsy diagnostics and therapy evaluation. Recent studies have shown that epileptiform discharges are connected with changes in the dynamics of the brain and possible alterations in connectivity between inter-connected areas of the brain. Transcranial magnetic stimulation (TMS) in combination with electroencephalogram (EEG) enables the non-invasive, direct study between brain areas. TMS induces an electrical field in the brain, causing a depolarization and generation of action potentials. The TMS-evoked EEG responses can be used to analyse the brain's excitability, the spread of activation and the brain network connectivity. [Filatova et al., 2018] demonstrated the potential of the Variational Bayesian Multimodal Encephalography (VBMEG) method to capture cortical source activity and estimate dynamic information flow in neural networks at the brain. The application of network analysis in epilepsy provides valuable information on the seizure onset, propagation and termination, on the interictal state of functional networks and on alterations in structural networks [Van Diessen et al., 2013].

Objective

Exploration of the VMBEG method of [Filatova et al., 2018] to map the (altered) connectivity network in subjects with epilepsy.

Study design

The medical files of patients referred for electroencephalography (EEG) diagnostics at the Epilepsy Monitoring Unit (EMU) in Stichting Epilepsie Instellingen Nederland (SEIN, location Heemstede), will be screened by neurologists involved in this study. Patients who meet the inclusion criteria, will be informed about the study by the neurologists. Participation consists of two sessions for subjects with temporal lobe epilepsy (TLE) patients (considered for epileptic surgery) and one session for both the subjects with genetic generalised epilepsy (GGE) and the healthy controls. During these sessions an EEG recording during a TMS stimulation protocol and a photic stimulation protocol will be performed. Using TMS predetermined regions in the motor cortex are activated. The TMS evoked response will be objectified using the EEG. This allows for non-invasive determination of the connectivity network. Lastly, a MRI-scan of the head will be made of all participants, enabling the projection of functional dynamic network changes on anatomical MRI tracts and areas.

Study population

- Temporal lobe epilepsy (TLE) patients (n=2), considered for epileptic surgery, whose anti- epileptic medication will be tapered, preferably to complete stop.
- Genetic generalised epilepsy (GGE) patients (n=2), who do not use any AED
- There will be an age-matched control group (n=2)

Intervention (if applicable)

Patients will undergo brain stimulation using single pulse TMS and photic stimulation during EEG recording. In addition, a MRI (T1 and diffusion weighted) will be performed.

Main study parameters/endpoints

The connectivity of the brain will be investigated by estimating the EEG activity of the cortical sources and the dynamic causal interactions between these. Exploration is focused on the question if this method is able to distinguished subjects with most likely generalised connectivity abnormalities from focal abnormalities, if both can be distinguished from healthy controls, and whether changes in anti-epileptic drug levels are reflected in measured network dynamics.

Nature and extent of the burden and risks associated with participation, benefit and group relatedness

Participation consists of two EEG recording appointments for the TLE patients and one appointments for both the genetic generalised epileptic (GGE) patients and the healthy control subjects. During each EEG recording session TMS and photic stimulation protocols will be performed with a total duration of 120 minutes. The first session for the TLE patients will be scheduled a week before the ad- mission to the EMU. The second session will be scheduled just before or directly after the EMU EEG recording, at the moment of lowest AED dosage. This scheduling ensures an undisturbed regular clinical EMU recording. Both GGE patients and healthy control subjects will make an appointment for one EEG session with TMS and photic stimulation protocols. In addition, all subjects will have another appointment for the MRI-scan. TMS is a safe technique. TMS stimulation itself can be experienced as a small shock due to an accompanying muscle twitch. During the stimulation protocol subject will be continuously monitored to determine comfort, tolerability, and effects of the stimulation trials. The first and most significant complication of TMS in literature is seizure induction in itself, especially when medication is being tapered (2.8% chance with regular TMS protocols) [Engel, 2008]. Our EEG-TMS setting as part of the EMU is a setting designed for optimal safety of patients in case of seizure events. Even in case of a seizure, the risk of complications is minimal. By doing measurements in both healthy controls and subjects with epilepsy, including with and without tapered medication, we will be exploring an objective method to study the brain network connectivity. The VBMEG method which was developed for stroke patients, showed promising results. If similar results can be found in subjects with epilepsy, this method van contribute to the understanding of the pathophysiology of epilepsy which will have a positive impact on the diagnostic process. Furthermore, in the future, it may help in determining the effect of the medication on the brain which might help choosing the right drug in future patients.

7.B Clinical history patients

Subject 3

Subject 3 is a 28 year old female with genetic generalised epilepsy. She was diagnosed may 2015. She suffered from tonic-clonic seizures until 2018, but still has daily absence seizures. Medication: Lamotrigine 500 mg/day and Brivaracetam 75 mg/day.

Subject 4

Subject 4 is a 23 year old female with diagnosed genetic generalised epilepsy. She was diagnosed early 2007. She suffers from absence seizures and occasionally tonic-clonic seizures. Medication: Lamotrigine 400 mg/day and Levetiracetam 2000 mg/day.

Subject 5

Subject 5 is a 38 year old man with a drug resistant focal epilepsy. He was diagnosed early 2009. He suffers from focal seizures both aware and with impaired awareness, sometimes the seizures expand from focal to bilateral generalised tonic-clonic seizures. Underlying aetiology might be a meningitis when he was 1 year old. MRI shows indications for a MTS in the left hemisphere. Medication: Carbamazepine 1400 mg/day, Clobazam 10 mg/day and Lacosamide 200 mg/day.

7.C Glasser HCP MMP 1.0 Atlas information

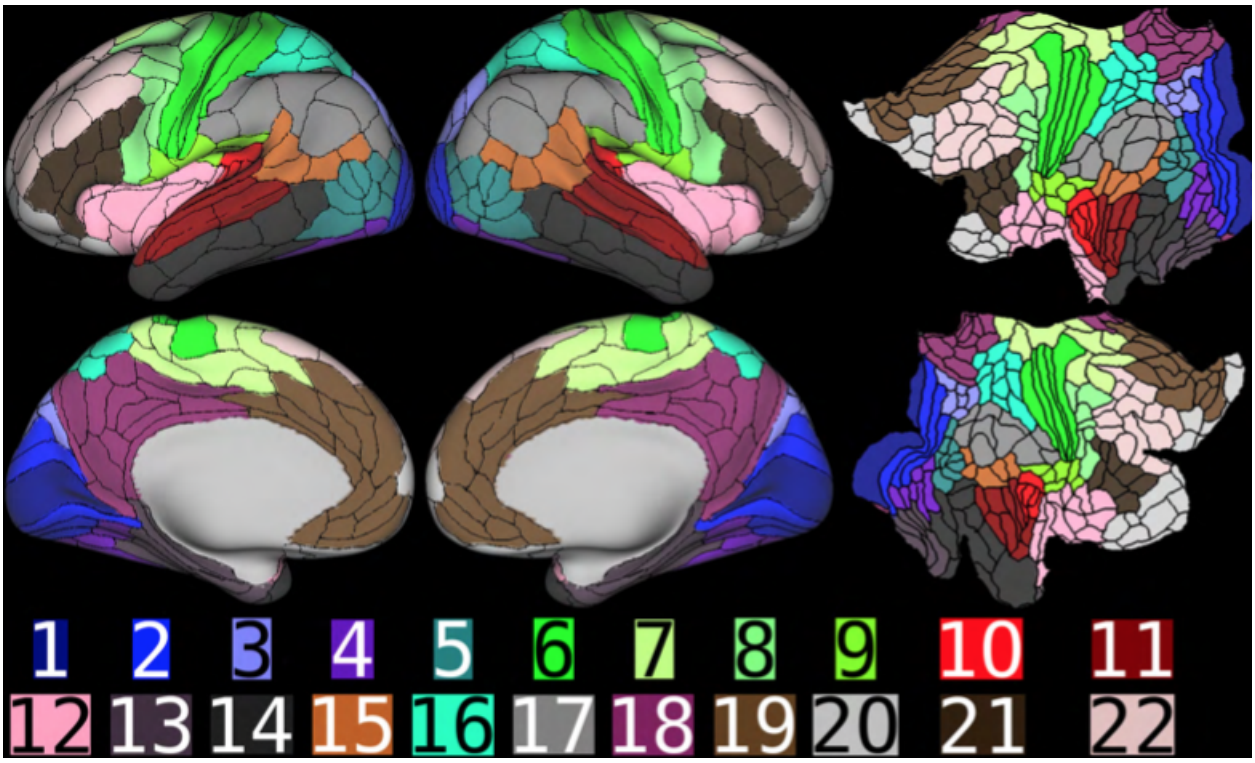

Figure 7: *Multimodal parcellation of Glasser*[Glasser et al., 2016]. The multimodel parcellation of Glasser. The 379 regions of interest are sub-divided into 21 regions based on on integrative information from cortical architecture (cortical thickness, myelin), function (task- fMRI), connectivity and/or topography (resting-state fMRI).

Table 7: The 21 regions of the HCP MMP 1.0 atlas, for more detailed information see [Glasser et al., 2016]

1	Primary visual cortex	**12**	Insular and Frontal Opercular Cortex
2	Early visual cortex	**13**	Medial Temporal Cortex
3	Dorsal stream cortex	**14**	Lateral Temporal Cortex
4	Ventral stream visual cortex	**15**	Temporo-Parieto-Occipital Junction
5	MT+ Complex and neighbouring visual areas	**16**	Superior Parietal Cortex
6	Somatosensory and motor cortex	**17**	Inferior Parietal Cortex
7	Paracentral Lobular and Mid Cingulate Cortex	**18**	Posterior Cingulate Cortex
8	Premotor cortex	**19**	Anterior Cingulate and medial prefrontal cortex
9	Posterior opercular cortex	**20**	Orbital and polar frontal cortex
10	Early auditory cortex	**21**	Inferior frontal cortex
11	Auditory association cortex		

7.D Additional results

Table 8: Mean FA values ± standard deviation per ROI per subject

Subject ID		1 (HC)	2 (HC)	3 (GGE)	4 (GGE)	5 (FE)
Cerebellum	Left	0.1815 ± 0.0922	0.1868 ± 0.0786	0.1753 ± 0.0921	0.1660 ± 0.0762	0.1561 ± 0.0848
	Right	0.1973 ± 0.1002	0.1972 ± 0.0768	0.1852 ± 0.0951	0.1809 ± 0.0758	0.1672 ± 0.1014
Thalamus	Left	0.3215 ± 0.1368	0.2863 ± 0.1092	0.2769 ± 0.1053	0.2775 ± 0.1028	0.2506 ± 0.0909
	Right	0.2764 ± 0.0951	0.2831 ± 0.1031	0.2578 ± 0.1076	0.2440 ± 0.0909	0.2510 ± 0.0950
Nucleus Caudutus	Left	0.2633 ± 0.1428	0.1972 ± 0.1064	0.2365 ± 0.1351	0.2698 ± 0.1412	0.2150 ± 0.1214
	Right	0.1760 ± 0.0974	0.1915 ± 0.1163	0.1761 ± 0.1126	0.1513 ± 0.0743	0.2008 ± 0.1077
Putamen	Left	0.2405 ± 0.1108	0.2114 ± 0.1091	0.2329 ± 0.1399	0.2371 ± 0.1177	0.2300 ± 0.1023
	Right	0.2743 ± 0.1571	0.2133 ± 0.1024	0.2581 ± 0.1571	0.2490 ± 0.1688	0.2496 ± 0.1020
Globus pallidus	Left	0.2411 ± 0.1297	0.3142 ± 0.1615	0.3685 ± 0.2169	0.3017 ± 0.1472	0.3417 ± 0.1930
	Right	0.4922 ± 0.2273	0.3315 ± 0.1517	0.4878 ± 0.2408	0.4716 ± 0.2267	0.3440 ± 0.1530
Hippocampus	Left	0.1620 ± 0.0757	0.1530 ± 0.0786	0.1597 ± 0.0917	0.1631 ± 0.0788	0.1422 ± 0.0687
	Right	0.1767 ± 0.1166	0.1490 ± 0.0777	0.1843 ± 0.1490	0.1753 ± 0.1133	0.1474 ± 0.0643
Amygdala	Left	0.1801 ± 0.0707	0.1754 ± 0.0619	0.1905 ± 0.0964	0.2058 ± 0.0825	0.1881 ± 0.0648
	Right	0.1782 ± 0.0854	0.1610 ± 0.0737	0.1906 ± 0.1203	0.1593 ± 0.0777	0.1758 ± 0.0619
Accumbens	Left	0.2965 ± 0.1856	0.2137 ± 0.0591	0.3464 ± 0.1924	0.2542 ± 0.1310	0.2476 ± 0.0902
	Right	0.2394 ± 0.1229	0.2200 ± 0.0632	0.2505 ± 0.1395	0.2017 ± 0.0844	0.2650 ± 0.1162
Ventral DC	Left	0.4339 ± 0.2044	0.3885 ± 0.2041	0.4554 ± 0.1949	0.3751 ± 0.1820	0.3791 ± 0.1772
	Right	0.4009 ± 0.1883	0.3979 ± 0.1997	0.4187 ± 0.1967	0.3598 ± 0.1873	0.3647 ± 0.1955
Brainstem		0.3778 ± 0.2113	0.3972 ± 0.1848	0.3898 ± 0.2057	0.3224 ± 0.1684	0.3360 ± 0.2108

Table 9: Mean mean diffusivity value with standard deviation ($10^{-3}mm^2/s$) per ROI per subject

Subject ID		1 (HC)	2 (HC)	3 (GGE)	4 (GGE)	5 (FE)
Cerebellum	Left	0.8431 ± 0.4946	0.8712 ± 0.3976	0.9329 ± 0.4954	0.9626 ± 0.5056	0.9114 ± 0.5652
	Right	0.8663 ± 0.4782	0.8379 ± 0.3612	0.9118 ± 0.4756	0.9140 ± 0.4420	0.9211 ± 0.5699
Thalamus	Left	0.7923 ± 0.1628	0.8692 ± 0.2715	0.9957 ± 0.4744	0.8641 ± 0.2952	0.9302 ± 0.3068
	Right	0.9929 ± 0.4805	0.8757 ± 0.3126	1.1245 ± 0.6154	1.0838 ± 0.5765	0.9860 ± 0.4342
Nucleus Caudutus	Left	0.7431 ± 0.1202	0.9073 ± 0.3707	0.7271 ± 0.0865	0.7769 ± 0.1284	0.9207 ± 0.3921
	Right	1.1809 ± 0.7349	0.9401 ± 0.3346	0.7004 ± 0.0627	1.3667 ± 0.7573	1.0420 ± 0.5339
Putamen	Left	0.7654 ± 0.1369	0.7339 ± 0.0721	0.7227 ± 0.1015	0.7537 ± 0.1481	0.7439 ± 0.0898
	Right	0.7158 ± 0.1124	0.7370 ± 0.0809	0.7004 ± 0.0627	0.7325 ± 0.1038	0.7271 ± 0.1232
Globus pallidus	Left	0.7884 ± 0.2115	0.7298 ± 0.0978	0.7227 ± 0.1015	0.7439 ± 0.1344	0.7505 ± 0.1094
	Right	0.6727 ± 0.0740	0.7347 ± 0.0934	0.6945 ± 0.0606	0.7008 ± 0.1119	0.7486 ± 0.1317
Hippocampus	Left	1.0394 ± 0.3049	1.1146 ± 0.4309	1.2510 ± 0.6212	1.0759 ± 0.3891	1.3313 ± 0.5702
	Right	1.1191 ± 0.4404	1.0691 ± 0.3581	1.1488 ± 0.4608	1.0827 ± 0.4626	1.1168 ± 0.4894
Amygdala	Left	0.9221 ± 0.2675	0.9557 ± 0.3042	1.0404 ± 0.4245	0.9807 ± 0.2997	0.8706 ± 0.1522
	Right	0.9477 ± 0.3628	1.0003 ± 0.3384	0.9912 ± 0.3521	1.0014 ± 0.3496	0.9301 ± 0.3700
Accumbens	Left	0.7679 ± 0.1205	0.9388 ± 0.3166	0.8156 ± 0.4231	0.8477 ± 0.2499	0.8076 ± 0.1107
	Right	0.8721 ± 0.2345	0.8934 ± 0.1988	0.8955 ± 0.3182	0.9632 ± 0.3141	0.9465 ± 0.4017
Ventral DC	Left	0.9087 ± 0.4195	0.9856 ± 0.4464	0.8530 ± 0.3329	0.9480 ± 0.3971	1.0226 ± 0.4762
	Right	0.9405 ± 0.4577	1.0100 ± 0.4952	0.9244 ± 0.4742	1.0021 ± 0.5022	1.1310 ± 0.6494
Brainstem		0.9883 ± 0.6724	1.0307 ± 0.5257	1.0347 ± 0.6255	1.1281 ± 0.6335	1.0378 ± 0.8029

Table 10: Mean radial diffusivity value with standard deviation($10^{-3}mm^2/s$) per ROI per subject.

Subject ID		**1 (HC)**	**2 (HC)**	**3 (GGE)**	**4 (GGE)**	**5 (HC)**
Cerebellum	Left	0.7614 ± 0.4728	0.7863 ± 0.3846	0.8479 ± 0.4795	0.8813 ± 0.4914	0.8355 ± 0.5403
	Right	0.7797 ± 0.4641	0.7503 ± 0.3481	0.8249 ± 0.4608	0.8305 ± 0.4336	0.8420 ± 0.5502
Thalamus	Left	0.6546 ± 0.1720	0.7383 ± 0.2612	0.8567 ± 0.4527	0.7386 ± 0.2759	0.8150 ± 0.3036
	Right	0.8603 ± 0.4615	0.7488 ± 0.3020	0.9868 ± 0.5965	0.9594 ± 0.5523	0.8653 ± 0.4223
Nucleus Caudutus	Left	0.6355 ± 0.1398	0.8177 ± 0.3694	0.8148 ± 0.4104	0.6600 ± 0.1464	0.8249 ± 0.3977
	Right	1.0826 ± 0.7024	0.8495 ± 0.3351	1.2684 ± 0.8089	1.2647 ± 0.7180	0.9440 ± 0.5140
Putamen	Left	0.6672 ± 0.1343	0.6510 ± 0.0822	0.6335 ± 0.0993	0.6561 ± 0.1442	0.6556 ± 0.0960
	Right	0.6052 ± 0.1317	0.6530 ± 0.0796	0.5979 ± 0.0922	0.6289 ± 0.1252	0.6336 ± 0.1190
Globus pallidus	Left	0.6952 ± 0.2085	0.6029 ± 0.1330	0.5618 ± 0.1611	0.6190 ± 0.1461	0.6040 ± 0.1644
	Right	0.4597 ± 0.1544	0.5963 ± 0.1221	0.4726 ± 0.1524	0.4938 ± 0.1831	0.6104 ± 0.1601
Hippocampus	Left	0.9510 ± 0.2841	1.0303 ± 0.4145	1.1496 ± 0.5888	0.9844 ± 0.3616	1.2396 ± 0.5432
	Right	1.0186 ± 0.4315	0.9886 ± 0.3444	1.0414 ± 0.4598	0.9859 ± 0.4530	1.0361 ± 0.4649
Amygdala	Left	0.8345 ± 0.2521	0.8694 ± 0.2916	0.9390 ± 0.4086	0.8753 ± 0.2917	0.7885 ± 0.1469
	Right	0.8553 ± 0.3265	0.9178 ± 0.3246	0.8919 ± 0.3485	0.9175 ± 0.3327	0.8502 ± 0.3564
Accumbens	Left	0.6423 ± 0.1643	0.8361 ± 0.2704	0.6822 ± 0.4403	0.7352 ± 0.2566	0.6996 ± 0.1014
	Right	0.7637 ± 0.2430	0.7990 ± 0.1875	0.7867 ± 0.3332	0.8651 ± 0.3063	0.8348 ± 0.3870
Ventral DC	Left	0.6934 ± 0.4469	0.7833 ± 0.4758	0.6299 ± 0.3582	0.7562 ± 0.4181	0.8247 ± 0.4921
	Right	0.7446 ± 0.4759	0.7990 ± 0.5183	0.7220 ± 0.5011	0.8236 ± 0.5261	0.9381 ± 0.6706
Brainstem		0.7941 ± 0.6593	0.8121 ± 0.5210	0.8271 ± 0.6325	0.9531 ± 0.6356	0.8585 ± 0.7797

Table 11: Mean axial diffusivity value with standard deviation ($10^{-3}mm^2/s$) per ROI per subject.

		1 (HC)	**2 (HC)**	**3 (GGE)**	**4 (GGE)**	**5 (FE)**
Cerebellum	Left	1.0067 ± 0.5455	1.0409 ± 0.4321	1.1028 ± 0.5346	1.1252 ± 0.5396	1.0632 ± 0.6207
	Right	1.0396 ± 0.5172	1.0130 ± 0.3960	1.0857 ± 0.5138	1.0810 ± 0.4675	1.0793 ± 0.6185
Thalamus	Left	1.0677 ± 0.2308	1.1310 ± 0.3310	1.2737 ± 0.5400	1.1151 ± 0.3647	1.1604 ± 0.3330
	Right	1.2580 ± 0.5378	1.1295 ± 0.3622	1.3999 ± 0.6752	1.3327 ± 0.6415	1.2274 ± 0.4729
Nucleus Caudutus	Left	0.9584 ± 0.1757	1.0865 ± 0.3934	1.1431 ± 0.4529	1.0109 ± 0.1836	1.1124 ± 0.4043
	Right	1.3775 ± 0.8137	1.1214 ± 0.3597	1.5960 ± 0.9140	1.5705 ± 0.8448	1.2382 ± 0.5885
Putamen	Left	0.9620 ± 0.1972	0.8996 ± 0.1361	0.9143 ± 0.1734	0.9487 ± 0.2139	0.9204 ± 0.1412
	Right	0.9371 ± 0.1989	0.9051 ± 0.1527	0.9055 ± 0.1799	0.9397 ± 0.2060	0.9142 ± 0.1816
Globus pallidus	Left	0.9748 ± 0.2432	0.9836 ± 0.1754	1.0446 ± 0.2569	0.9938 ± 0.2200	1.0434 ± 0.1944
	Right	1.0987 ± 0.2530	1.0114 ± 0.1803	1.1383 ± 0.2764	1.1147 ± 0.2241	1.0251 ± 0.1883
Hippocampus	Left	1.2162 ± 0.3685	1.2832 ± 0.4783	1.4538 ± 0.7049	1.2590 ± 0.4628	1.5146 ± 0.6352
	Right	1.3200 ± 0.4951	1.2300 ± 0.4035	1.3635 ± 0.5138	1.2764 ± 0.5110	1.2780 ± 0.5470
Amygdala	Left	1.0975 ± 0.3151	1.1281 ± 0.3403	1.2434 ± 0.4813	1.1916 ± 0.3377	1.0350 ± 0.1846
	Right	1.1327 ± 0.4624	1.1654 ± 0.3833	1.1898 ± 0.4096	1.1693 ± 0.4027	1.0900 ± 0.4047
Accumbens	Left	1.0190 ± 0.2049	1.1442 ± 0.4189	1.0824 ± 0.4294	1.0727 ± 0.3078	1.0237 ± 0.1799
	Right	1.0890 ± 0.2693	1.0822 ± 0.2408	1.1131 ± 0.3205	1.1595 ± 0.3472	1.1699 ± 0.4535
Ventral DC	Left	1.3394 ± 0.4614	1.3903 ± 0.4749	1.2990 ± 0.3964	1.3316 ± 0.4284	1.4184 ± 0.4995
	Right	1.3323 ± 0.4872	1.4319 ± 0.5266	1.3292 ± 0.4857	1.3590 ± 0.5084	1.5168 ± 0.6526
Brainstem		1.3766 ± 0.7457	1.4679 ± 0.5953	1.4499 ± 0.6680	1.4783 ± 0.6642	1.3963 ± 0.8842

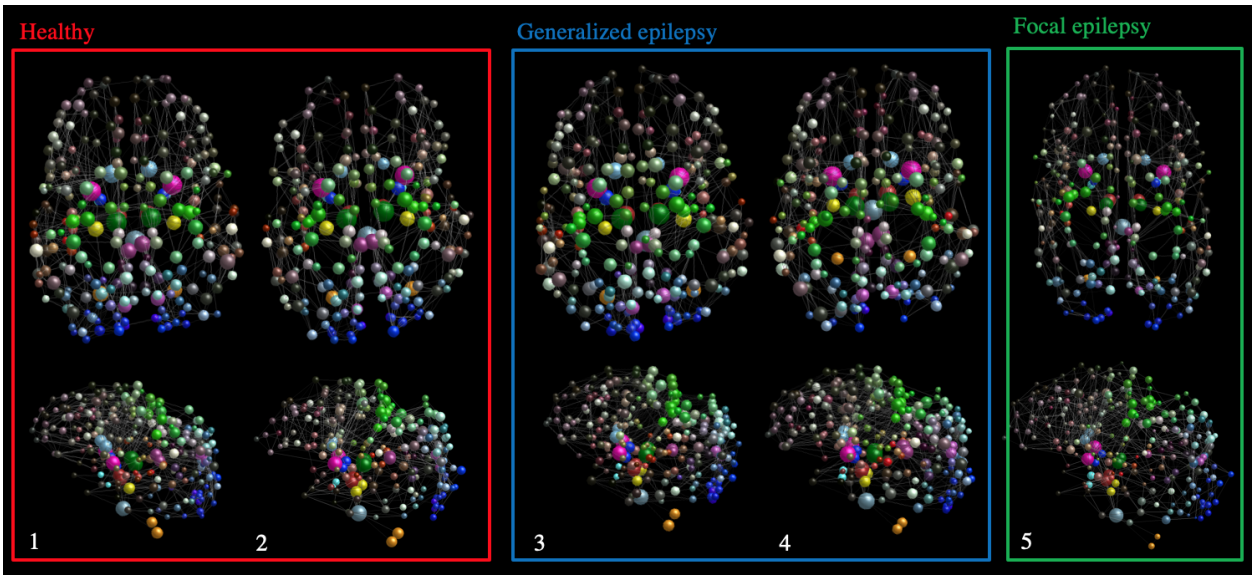

Figure 8: *Overview of the structural connectome per subject.* The image shows the structural connectome of each of the subjects, nodes are scaled based on their node degree. The colours correspond to the [Glasser et al., 2016] atlas. A decreased overall node degree is seen in subject 5, and a decreased node degree is seen in the visual cortex in both subject 4 and 5. This can be explained as a decreased connectivity.

7.E Workflow of data analysis

The figure shows a schematic overview of the workflow of the data analysis as is performed in this study. The workflow is based on the VBMEG method (`https://vbmeg.atr.jp`). Preprocessing of the T1-weighted MRI's is done in SPM8 (`https://fil.ionucle.ac.uk/spm/`), cortical reconstruction is done with the Freesurfer suite v6.0 (`https://surfer.nmr.mgh.harvard.edu`). Cortical parcellation is according to the HCP MMP 1.0 atlas ([Glasser et al., 2016]), subcortical structures are segmentented automatically in the Freesurfer suite. Preprocessing of the diffusion MRI' in FSL v6.0, the tractography in MRTrix v3.0 (`https://www.mrtrix.org`) and the network analysis with the use of the brain connectivity toolbox ([Rubinov and Sporns, 2010]) and network based statistics ([Zalesky et al., 2010]). Adjustments have been made based on the MRtrix documentation, forum and the BATMAN Tutorial from [Tahedi, 2018]. The workflow starts with preprocessing (yellow), followed by ROI analysis (light blue), probabilistic tractography (dark blue), tract density maps of the thalamo-cortical radiations (red) and network analysis (pink). Endpoints are indicated by the filled coloured boxes. CSD = Constrained Spherical Deconvolution, ACT = Anatomically constraint tractography, MSMT = Multi Shell Multi Tissue, iFOD2 = Second-order Integration over Fiber Orientation Distributions, SIFT = Spherical Deconvolution Informed Filtering of Tracts.

The caption is removed from the last page, to make sure the workflow entails the whole page to improve readability.

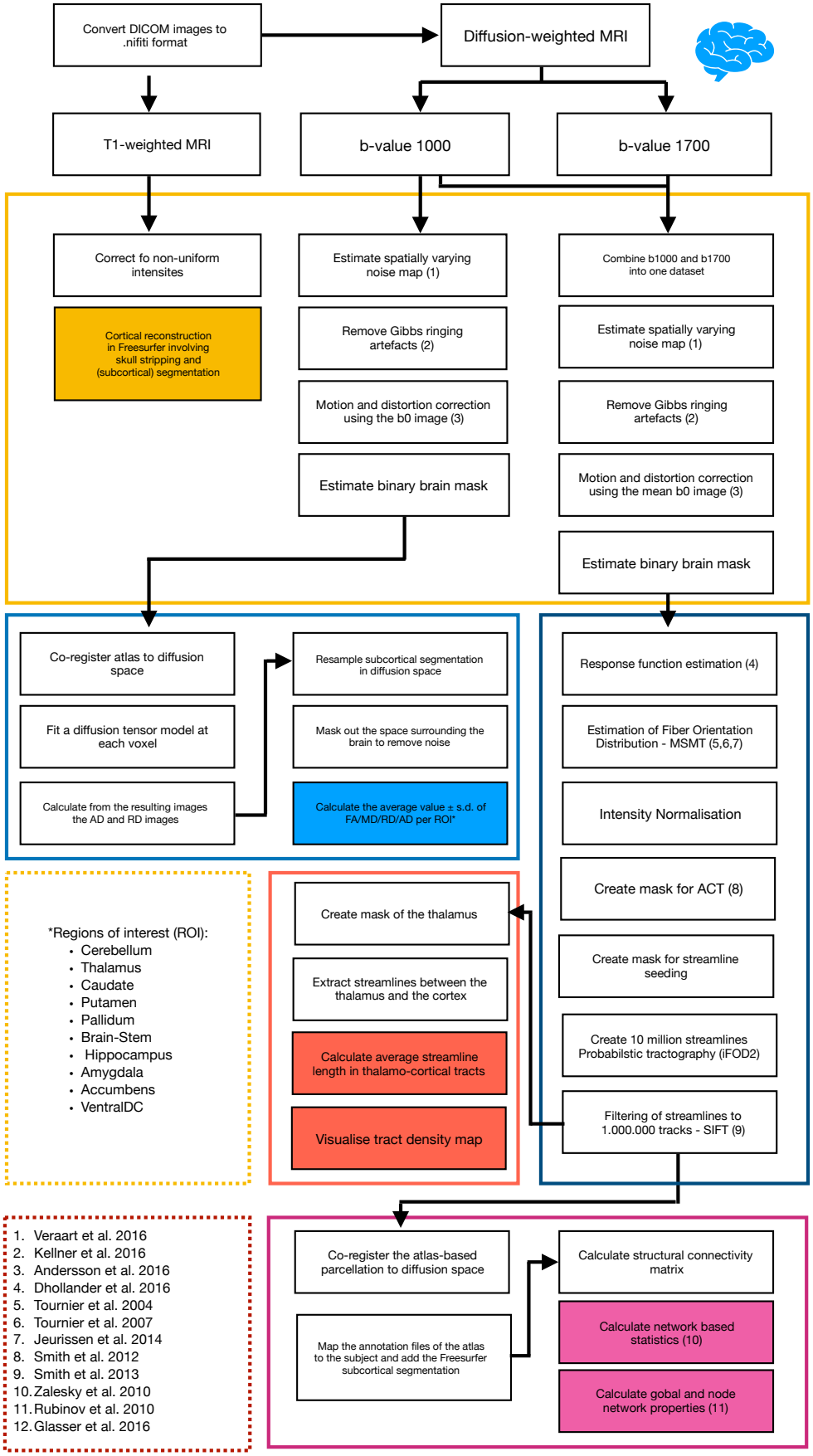
Convert DICOM images to .nifiti format
Diffusion-weighted MRI
T1-weighted MRI
b-value 1000
b-value 1700
Correct fo non-uniform intensites
Cortical reconstruction in Freesurfer involving skull stripping and (subcortical) segmentation
Estimate spatially varying noise map (1)
Remove Gibbs ringing artefacts (2)
Motion and distortion correction using the b0 image (3)
Estimate binary brain mask
Combine b1000 and b1700 into one dataset
Estimate spatially varying noise map (1)
Remove Gibbs ringing artefacts (2)
Motion and distortion correction using the mean b0 image (3)
Estimate binary brain mask
Co-register atlas to diffusion space
Fit a diffusion tensor model at each voxel
Calculate from the resulting images the AD and RD images
Resample subcortical segmentation in diffusion space
Mask out the space surrounding the brain to remove noise
Calculate the average value ± s.d. of FA/MD/RD/AD per ROI*
Response function estimation (4)
Estimation of Fiber Orientation Distribution - MSMT (5,6,7)
Intensity Normalisation
Create mask for ACT (8)
Create mask for streamline seeding
Create 10 million streamlines Probabilstic tractography (iFOD2)
Filtering of streamlines to 1.000.000 tracks - SIFT (9)
*Regions of interest (ROI):
Cerebellum
Thalamus
Caudate
Putamen
Pallidum
Brain-Stem
Hippocampus
Amygdala
Accumbens
VentralDC
Create mask of the thalamus
Extract streamlines between the thalamus and the cortex
Calculate average streamline length in thalamo-cortical tracts
Visualise tract density map
1. Veraart et al. 2016
2. Kellner et al. 2016
3. Andersson et al. 2016
4. Dhollander et al. 2016
5. Tournier et al. 2004
6. Tournier et al. 2007
7. Jeurissen et al. 2014
8. Smith et al. 2012
9. Smith et al. 2013
10. Zalesky et al. 2010
11. Rubinov et al. 2010
12. Glasser et al. 2016
Co-register the atlas-based parcellation to diffusion space
Map the annotation files of the atlas to the subject and add the Freesurfer subcortical segmentation
Calculate structural connectivity matrix
Calculate network based statistics (10)
Calculate gobal and node network properties (11)